Physics and Thermodynamics of Capillary

A thermodynamic theory and a detailed mechanism of immiscible displacement in porous media are developed in terms of a quantized model

A wide range of natural and technological processes involves capillary action associated with immiscible fluid displacement within the interstices of porous solids. Examples are the movement of air and water in soils and porous rocks, the recovery of hydrocarbons from subterranean reservoirs, the drying, centrifuging and dewatering of porous solids, the behavior of porous fuel cell electrodes, and the capillary properties of textile and paper fibers.

Although principles of capillary action are well understood, their application to practical problems is often limited by the complicated geometry of porous solids. Difficulties are compounded when there is uncertainty as to the surface energetics of the system which determine the property generally described as the wettability of a porous solid.

The structure and surface properties of numerous types of porous materials are commonly investigated by measurement of capillary displacement pressures as a function of displaced volume. Often it has been assumed that immiscible displacement can be treated as a smoothly reversible process. Thermodynamic relationships based on this assumption have been used to relate the work of displacement to changes in the area of the surfaces which bound the fluid phases contained by the solid. Although so-called capillary pressure equilibrium points appear to be part of a continuous relationship between capillary pressure and displaced volume, these relationships are not reversible. Furthermore, when examined in fine detail, they are not continuous. Much of the confusion surrounding the thermodynamic interpretation of capillary pressure data can be avoided by giving consideration to the frequently referenced general treatment of capillarity by J. W. Gibbs (*1*) and the investigations of displacement in porous solids by W. B. Haines (*2*).

This paper has three main sections. In the first section, the terminology used in discussing surface energetics is defined, and thermodynamic relationships for reversible displacements are derived from fundamental thermodynamic equations. In the second section, the mechanism and thermodynamics of displacement in porous media are discussed. To obtain infinitesimally slow displacement in porous media, special conditions are required which lead to a quantized model of displacement. Changes in volumetric and surface quantities can be classified within the framework of the quantized model to give a consistent account of the displacement mechanism. The third section describes an experimental investigation of displacement in random packings of equal-sized spheres, commonly known as the ideal soil. Changes in surface area of phases within the packings are measured directly to obtain the changes of free energy due to surface. Inherent thermodynamic efficiencies of displacement are then obtained by comparing changes in surface free energy with the work of displacement given by capillary pressure data.

SURFACE ENERGETICS

There is no generally accepted terminology by which surface energetics can be discussed without risk of ambiguity to the reader. The following terms have appeared in published literature (*1–10*): surface tension, superficial tension, interfacial tension, adhesion tension,

AUTHOR *Norman R. Morrow is Senior Research Scientist with the Petroleum Recovery Research Institute, The University of Calgary, Calgary, Alta., Canada.* *The author expresses his appreciation to J. O. Szabo for valuable assistance in preparation of thin sections and to Esso Production Research Co. for permission to publish. This paper was presented as part of the Symposium on Flow Through Porous Media, The Carnegie Institution, Washington, D. C., June 9–11, 1969.*

Figure 1. Gibbs model of surface between two fluids

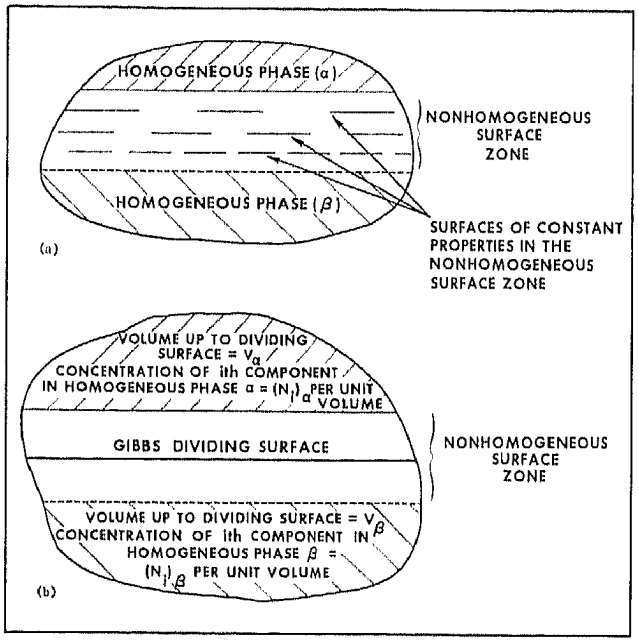

Action in Porous Media

NORMAN R. MORROW

surface stress, stress tension, surface free energy, superficial densities of energy, specific surface energy, free surface energy, surface energy, surface energy density, Helmholtz free energy, surface Helmholtz free energy, specific surface free energy, pure surface energy, real surface energy, actual surface energy, theoretical free surface energy, free energy of formation, and relative surface free energy.

The terms surface tension, surface free energy, and superficial surface free energy will first be defined as used in this paper. The last term is defined to preclude any possible misunderstanding of the term surface free energy. We will begin by defining and comparing the above three terms as they relate to a system of two fluid phases, α and β, separated by a plane interface, S, of area A. In subsequent discussions, several pairs of fluids will be used as wetting and nonwetting phases with respect to a solid. The nomenclature will be defined as each pair is introduced, but for convenience in future references, they are listed in Table I.

Surfaces between Fluids

Superficial surface free energy. The physical surface of discontinuity is viewed as a nonhomogeneous film separating two homogeneous phases. The properties of the film vary along normals to the surface but are constant over any geometrical surface which is parallel to the physical surface (Figure 1a). Gibbs (*11*) introduced a mathematical model whereby thermodynamic quantities, which he termed superficial, could be assigned to the regions α and β and a geometrical surface which divides these regions (Figure 1b). The geometrical dividing surface lies in and is sensibly coincident with the physical surface of discontinuity (Figure 1b). All points in the mathematical surface are similarly situated with respect to the physical surface. The precise position of the Gibbs dividing surface is arbitrary, but, of course, all possible placements lie parallel to each other.

The geometrical surface precisely divides the volume, V, of the system into regions α and β with V_α, the volume

Table I. Nomenclature for Three-Phase Systems (Solid-wetting phase–nonwetting phase)

System fluids	Notation: Solid area, A_s	Notation: Wetting phase	Notation: Nonwetting phase	Pore space saturations: Wetting phase	Pore space saturations: Nonwetting phase	Surface areas between phases: Wetting-nonwetting	Surface areas between phases: Wetting solid	Surface areas between phases: Nonwetting solid
General	s	α	β	S_α	S_β	$A_{\alpha\beta}$	$A_{s\alpha}$	$A_{s\beta}$
Water–oil	s	w	o	S_w	S_o	A_{wo}	A_{sw}	A_{so}
Water–air	s	w	a	S_w	S_a	A_{wa}	A_{sw}	A_{sa}
Water–vapor	s	w	v	S_w	S_v	A_{wv}	A_{sw}	A_{sv}
Liquid–air	s	l	a	S_l	S_a	A_{la}	A_{sl}	A_{sa}
Liquid–vapor	s	l	v	S_l	S_v	A_{lv}	A_{sl}	A_{sv}

A = area, s = solid, w = water, o = oil, a = air, v = vapor, l = liquid.

associated with the α phase, and V_β, the volume associated with the β phase (see Figure 1b)

$$V = V_\alpha + V_\beta \tag{1}$$

The essential feature of the mathematical model is that bulk properties of each phase are maintained right up to the dividing surface. Let the number of moles per unit volume of the ith component be $(N_i)_\alpha$ and $(N_i)_\beta$ in the homogeneous parts of the α and β phases, respectively. Molar quantities for the regions α and β up to the dividing surface of the Gibbs model are given by

$$(n_i)_\alpha = (N_i)_\alpha V_\alpha \tag{2}$$

$$(n_i)_\beta = (N_i)_\beta V_\beta \tag{3}$$

If the total number of moles of component i in the system is n_i, a material balance defines a surface excess (or deficiency) of, say, the ith component which will be denoted by $(n_i)_S$

$$n_i = (n_i)_\alpha + (n_i)_\beta + (n_i)_S \tag{4}$$

Similarly, if F is the total Helmholtz free energy of the system, F_α is the Helmholtz free energy of a volume V_α of the α phase in bulk, and F_β is the Helmholtz free energy of a volume V_β of the β phase in bulk, a superficial surface free energy, F_S, of the surface is defined by

$$F = F_\alpha + F_\beta + F_S \tag{5}$$

The fundamental Gibbs equation for change in Helmholtz free energy of a system with j components is

$$dF = -S'dT + \sum_{i=1}^{j} \mu_i dn_i - P_\alpha dV_\alpha - P_\beta dV_\beta + \sigma dA_{\alpha\beta} \tag{6}$$

The intensive quantities given in the right-hand side of Equation 6 are entropy, chemical potential, pressure, and surface tension, respectively.

When changes are isothermal, for the two regions α and β, we may write

$$dF_\alpha = \sum_{i=1}^{j} \mu_i d(n_i)_\alpha - P_\alpha dV_\alpha \tag{7}$$

$$dF_\beta = \sum_{i=1}^{j} \mu_i d(n_i)_\beta - P_\beta dV_\beta \tag{8}$$

Change in superficial surface free energy F_S is given by

$$dF_S = dF - dF_\alpha - dF_\beta \tag{9}$$

From Equations 6–9,

$$dF_S = \sum_{i=1}^{j} \mu_i dn_i - \sum_{i=1}^{j} \mu_i d(n_i)_\alpha - \sum_{i=1}^{j} \mu_i d(n_i)_\beta + \sigma dA_{\alpha\beta} \tag{10}$$

From Equation 4

$$d(n_i)_S = dn_i - d(n_i)_\alpha - d(n_i)_\beta \tag{11}$$

Hence, writing A for $A_{\alpha\beta}$,

$$dF_S = \sum_{i=1}^{j} \mu_i d(n_i)_S + \sigma dA \tag{12}$$

Let the total area of the surface, S, be A and the surface excess per unit area of component i, as determined by the model, be Γ_i, thus

$$(n_i)_S = \Gamma_i A \tag{13}$$

$$d(n_i)_S = \Gamma_i dA + A d\Gamma_i \tag{14}$$

From Equation 12,

$$dF_S = \sum_{i=1}^{j} \mu_i \Gamma_i dA + \sum_{i=1}^{j} \mu_i A d\Gamma_i + \sigma dA \tag{15}$$

$$\left(\frac{\partial F_S}{\partial A}\right)_{T,V,n} = \sum_{i=1}^{j} \mu_i \Gamma_i + \sum_{i=1}^{j} \mu_i A \left(\frac{\partial \Gamma_i}{\partial A}\right)_{T,V,n} + \sigma \tag{16}$$

where the subscript n implies that the number of moles of each component, $i = 1$ to j, is constant.

Variation of Γ_i with surface area will occur if, say, one component resides only in the surface and not in the contiguous bulk masses. In theory, the surface could be supplied with this component so that the properties of the surface per unit area remain constant.

When the properties of the surface per unit area are independent of the total area,

$$\left(\frac{\partial \Gamma_i}{\partial A}\right)_{T,V,n} = 0 \tag{17}$$

Integration of Equation 16 then gives

$$\frac{F_S}{A} = \sum_{i=1}^{j} \mu_i \Gamma_i + \sigma \tag{18}$$

Let the superficial surface free energy per unit area be f_S defined by

$$f_S = \sum_{i=1}^{j} \mu_i \Gamma_i + \sigma \tag{19}$$

Recall that the location of the dividing surface which determines the magnitude of Γ_i and f_S is arbitrary. The dividing surface is sometimes placed so that $\Gamma_i = 0$ for one component. For the single component system given by a pure liquid and its vapor, the dividing surface can be located so that $\Gamma = 0$ and then

$$f_S = \sigma \tag{20}$$

However, in general, the surface tension, which is numerically equal to the reversible work of extension per unit area of surface, is not equal to the superficial surface free energy.

Surface free energy and surface tension. From Equation 6, surface tension is defined by

$$\left(\frac{\partial F}{\partial A}\right)_{T,V,n} = \sigma \tag{21}$$

If the surface tension is constant,

$$(\Delta F)_{T,V,n} = \sigma \Delta A \tag{22}$$

Let the increase in Helmholtz free energy of the system due to a unit of area extension be f, then

$$\left(\frac{\Delta F}{\Delta A}\right)_{T,V,n} = f \tag{23}$$

Hence

$$\sigma = f \tag{24}$$

and from Equation 19, f and f_S are related by

$$f_S = \sum_{i=1}^{j} \mu_i \Gamma_i + f \tag{25}$$

The change in free energy of the system, $(\Delta F)_{T,V,n}$, is equal to the reversible work of extension of the surface. Gibbs described the product $\sigma \Delta A$, given by Equation 22 above, as the available energy due to the surface in the system (*13*). In many discussions of capillarity, the product, $\sigma \Delta A$, has been called surface free energy, and we shall follow that practice here. We do this somewhat reluctantly because Defay and Prigogine have called the quantity f_S the surface free energy. They describe confusion between surface tension and what they call surface free energy as particularly illogical (*14*). Johnson (*7*) points out that the term surface free energy is often used without further definition. In the majority of these instances, we believe the term surface free energy is intended to mean f, the free energy of the system due to the presence of the surface; this is particularly so if the Gibbs mathematical dividing surface has not been introduced.

In systems where the surface tension is dependent upon surface area, the surface free energy, as we have defined it, will not be equal to the product of surface tension and area. The change in surface free energy due to a change in area from A_1 to A_2 is now given by

$$(\Delta F)_{T,V,n} = \int_{A_1}^{A_2} \sigma(A) dA \tag{26}$$

Also, the surface free energy due to a unit area of surface, f, will depend upon the magnitude of the area and is not equal to the surface tension. Systems containing insoluble surfactants provide examples where the surface tension may vary significantly with area because surfactant concentration and the related spreading pressure of the surfactant depend upon absolute area. Such variations are commonly investigated experimentally with some form of surface tension trough (*3*).

Surface curvature and location of dividing surface. A completely general discussion of capillarity would require consideration of the effect of curvature on both surface tension and the location of the Gibbs reference surface which lies within the physical surface. However, these effects do not become significant until radii of curvature of a surface approach molecular dimensions (*15–17*). In porous media which are reasonably permeable to fluid flow, the curvatures of surfaces between fluids given by displacement pressures are relatively low. Thus the previous discussion of the energetics of plane surfaces extends to fluid interfaces developed during immiscible displacement.

Surface Energetics of Systems Containing Solid Surfaces

The conceptual difficulties involved in treating the surface energetics of solids are generally admitted.

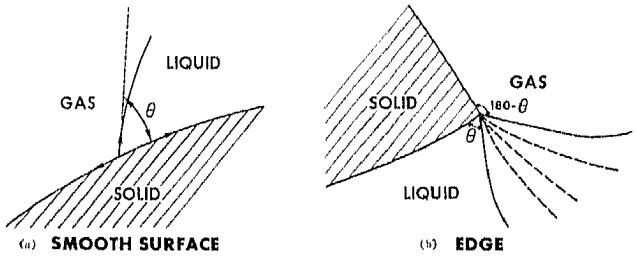

Figure 2. Equilibrium at a three-phase line of contact

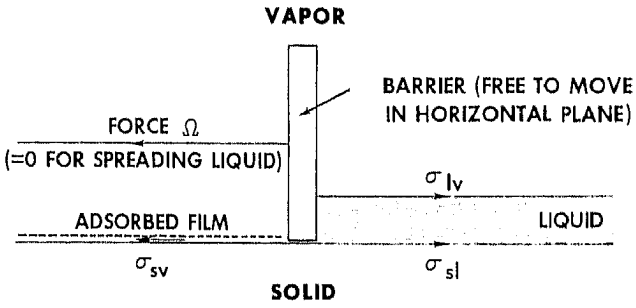

Figure 3. Hypothetical model illustrating stability for plane liquid and adsorbed film surfaces

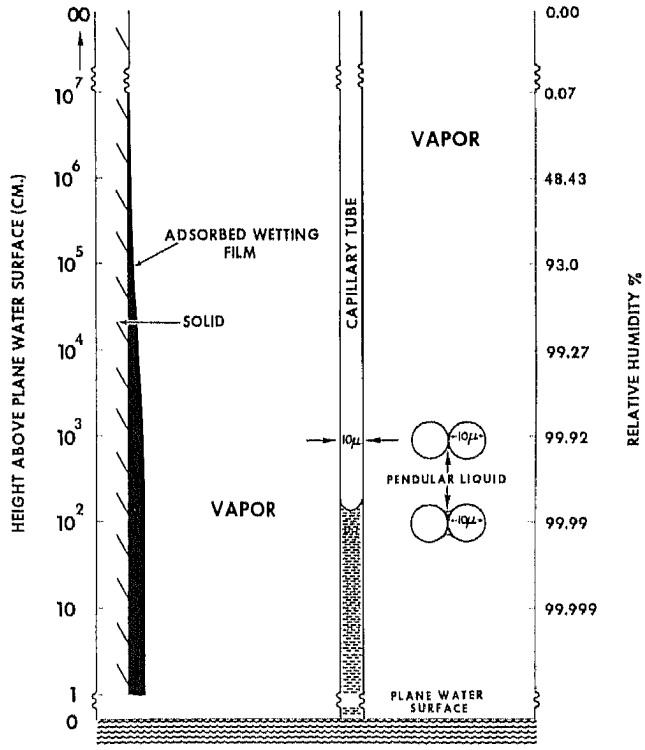

Figure 4(a). Equilibrium of adsorbed surface film and capillary-held liquid

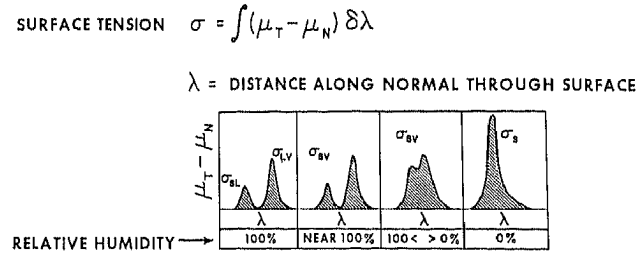

Figure 4(b). Sketches of variation in stress anisotropy with height for adsorbed film depicted in Figure 4a

Treatments of multiphase systems containing solids are found in the original work of Gibbs (*1*) and the more recent work of Defay and Prigogine (*18*). These general treatments will be tailored to the needs of the present development. Three-phase systems in which one of the phases is a solid will be considered first.

A complication of dealing with solids is that the state of strain of the solid in the region of the surface may be important. With fluids, surface tension acts uniformly in the surface, independent of direction, and can be measured directly as a force. In a crystalline solid with anisotropic elastic properties, surface tension cannot be measured directly, but the force required to stretch the surface infinitesimally may vary with direction in the surface.

Gibbs (*19*) defined a quantity, σ, as the work required to form a unit area of the surface, with the assumption that the properties of the surface are directly proportional to the area of the surface. Gibbs defined σ in terms of *integral* excess properties of the surface.

$$\sigma = f_S - \sum_{i=2}^{j} \mu_i \Gamma_i \tag{27}$$

The dividing surface was chosen to make the surface excess of the solid (component 1) equal to zero. In this way, the problems arising from variations in chemical potential with state of strain of anisotropic solids are circumvented.

We can also define σ as the contribution to the total Helmholtz free energy of the system due to the presence of a unit area of the surface in question. In other words, σ is the reversible work of formation of the surface

$$\sigma = \left(\frac{\Delta F}{\Delta A}\right)_{T,V,n} \tag{28}$$

If the state of stress is isotropic, σ is also equal to the surface tension. In accordance with the proposed terminology for fluid interfaces, σ will be called the surface free energy per unit area. (With regard to the problem of terminology, Defay and Prigogine call σ of Equation 27 the surface tension by analogy with the definition of σ of Equation 19 for fluid interfaces. They name the quantity f_S, as given by Equation 27, the relative surface free energy, where we suggest the name superficial surface free energy by analogy with Equation 19.)

Defay and Prigogine point out that one of the disadvantages of working in terms of σ as the free energy of formation is the practical difficulty of measuring the external work done in forming a solid-fluid surface by an isothermal and reversible process. This problem is absent for systems of interest here, since we consider only changes in surface free energy which accompany displacement of one overlying fluid by another from a solid surface assumed to maintain constant surface area. The reversible work of displacement of a three-phase line of contact across the solid surface will be given by the product of the changes in area and the difference in the two σ quantities of the solid surface.

Equilibrium at three-phase line of contact—Young's equation. It is frequently observed that the interface between two fluid phases meets an apparently smooth surface of a solid phase, s, at a finite angle, say θ, measured through the wetting phase as shown in Figure 2a.

In the region of the three-phase line of contact given by such a system, the model which enabled us to define a dividing surface within the physical surface breaks down. However, the selected dividing surfaces can be extrapolated into the three-phase confluent zone. The dividing surfaces will define exact surface areas between phases, and a mathematical line to which line excess quantities can be assigned (*20*). For example, the excess of the ith component with respect to the three-phase line of contact, $(n_i)_L$ is given by

$$n_i = (n_i)_\alpha + (n_i)_\beta + (n_i)_s + (n_i)_{S(\alpha\beta)} + (n_i)_{S(s\alpha)} + (n_i)_{S(s\beta)} + (n_i)_L \tag{29}$$

For the systems of interest here, the region occupied by the three-phase line of contact contains few molecules compared with the other surface regions. The contribution to the Helmholtz free energy of the system due to variation in the length of the three-phase line of contact, which may result from variation in surface areas, can therefore be neglected.

If we assume that the solid is smooth and rigid and that θ is single valued, the condition for thermodynamic equilibrium along the three-phase line of contact is given by Gibbs (*21*) as

$$\sum_{k=1}^{3} (\sigma_k \delta\tau) dx \geq 0 \tag{30}$$

where σ_k = surface free energy per unit area of the kth surface
$\delta\tau$ = element taking along the three-phase line of contact
dx = infinitesimal displacement over the solid surface normal to the element, $\delta\tau$

Let the surface area between the phases be A, with appropriate subscripts used to define a particular surface.

$$dA_{s\alpha} = \delta\tau dx \tag{31}$$

$$dA_{s\beta} = -\delta\tau dx \tag{32}$$

$$dA_{\alpha\beta} = \delta\tau dx \cos\theta \tag{33}$$

Hence, from Equation 30,

$$\sigma_{\alpha\beta} \cos\theta + \sigma_{s\alpha} - \sigma_{s\beta} = 0 \tag{34}$$

A more general derivation of this equation with gravitational potential and surface free energy minimized has been given by Collins and Cooke (*22*).

Equation 34 relates the difference in two quantities, $\sigma_{\beta s}$, $\sigma_{\alpha s}$, which cannot be measured individually, to the quantities $\sigma_{\alpha\beta}$ and θ which can be measured and is the equivalent of Young's equation (*23*). This equation is often presented on the basis of a simple force balance. For equilibrium, the fluid surface tension resolved in the plane of the solid surface must be balanced by some type of force acting in the surface. If the forces acting

in the plane of the solid surface and normal to the three phase line of contact are denoted by γ, we obtain

$$\sigma_{\alpha\beta} \cos \theta = \gamma_{\beta s} - \gamma_{\alpha s} \quad (35)$$

Severe conceptual difficulties concerning the nature of the γ quantities offset the apparent simplicity of this relationship. These difficulties have led to several disagreements as to the interpretation and validity of Young's equation. A consistent interpretation of Young's equation, which includes the special case of zero contact angle, is given by Gibbs. Before discussing Gibbs treatment, two examples where Young's equation may not be appropriate in its above form will be mentioned.

Deformation of solid surfaces. The vertical component of tension between the fluids, $\sigma_{\alpha\beta} \sin \theta$, is balanced by forces which cause the solid to be strained. For example, deformation of solid surfaces along the three-phase line of contact is described for mercury on mica (*24*). When the modulus of elasticity is low, Lester calculated that the solid will deform to give a ridge along the three-phase line of contact. In such cases, the Neumann surface tension triangle for three fluids should be used to express the balance of forces at the three-phase line of contact, rather than Young's equation (*25*).

Spreading of solid substrates. If the solid is partially soluble in either of the fluid phases, adsorption may cause a significant reduction in the surface tension, $\sigma_{\alpha\beta}$, observed for the two fluids alone. Thus, measurements of $\sigma_{\alpha\beta}$ may not always be applicable to the equilibrium expressed by Equation 34. Fowkes (*26*) estimated the spreading pressure, π_L, of solids or possible atmospheric contaminants on a mercury-air interface by comparing measured contact angles with those calculated for a mercury-air surface tension of 484 dynes/cm with $\pi_L = 0$. The contact angles were calculated from interaction energies which had in turn been estimated from surface tension measurements on standard systems. Using liquid advancing and receding contact angle data, estimates of the spreading pressure of solids on mercury ranged from 45.5 dynes/cm for paraffin wax to 100.5 dynes/cm for polyethylene.

Gibbs formulation of Young's equation—the unchangeable solid. Gibbs (*27*) introduced the unchangeable solid as a model. The unchangeable solid is insoluble in the fluid phases and its state of strain when bounded by a vacuum is unaltered by the presence of an overlying fluid. Properties of the unchangeable solid will be assumed in all subsequent discussion of solids including porous media.

The superficial tension of the fluid, η, is given by the tension in the solid-fluid interface, $\sigma_{s\alpha}$, less the tension in the solid surface when it is bounded by a vacuum, σ_s.

$$\eta_{s\alpha} = \sigma_{s\alpha} - \sigma_s \quad (36)$$

In effect, the model divides the surface tension at the solid-fluid interface $\sigma_{s\alpha}$, into the two components, $\eta_{s\alpha}$ and σ_s. Under the stated conditions, the fluid has no influence on the disposition of the solid; but the presence of the solid does influence the contractile forces within the fluid to give rise to $\eta_{s\alpha}$, which Gibbs named the superficial tension of the fluid in contact with the solid. When the system is in equilibrium, a balance of forces along a tangent to the solid surface at, and normal to, the three-phase line of contact gives

$$\eta_{s\beta} + \sigma_s = \eta_{s\alpha} + \sigma_s + \sigma_{\alpha\beta} \cos \theta \quad (37)$$

Hence,

$$\eta_{s\beta} - \eta_{s\alpha} = \sigma_{\alpha\beta} \cos \theta \quad (38)$$

Melrose (*28*) points out that the quantity, η, with opposite sign, is equal to the more commonly encountered film pressure. For example, when a drop of liquid on a smooth solid surface is in equilibrium with its vapor, the tension in the vapor solid surface is given by the tension of the solid surface in vacuum less the film pressure of the adsorbed vapor on the solid surface.

Stability in systems containing solid edges. As in the treatment of surfaces between two fluids, the preceding discussion, which includes solids, applies strictly to plane surfaces. However, as with curved liquid surfaces, the effects of curvature on surface free energy can probably be safely neglected for smooth solid surfaces.

Many natural solids, especially if freshly broken, have regions of extremely high curvature. As a limiting case, without considering the question of smoothness at a molecular level, the solid can be regarded as having smooth surfaces which may be wholly or partially bounded by edges. Gibbs (*27*) considered the conditions for equilibrium at a three-phase (two fluids and a solid) line of contact for the two cases of smooth surfaces and edges. The simpler case of the smooth solid is given by Equation 34. In contrast, for equilibrium at an edge, the angles at which the interface between the fluids can possibly meet one of the edges forming the surface, cover a range which is determined by the angle subtended at the edge by the two solid surfaces. The range of angles through which a three-phase line of contact can be observed at an edge, provided other requirements of stability are met, is depicted in Figure 2b. Clearly, the contact angle condition for stability of an interface between two fluids in the presence of a solid has been relaxed. As a consequence, in systems containing angular solids, most of the three-phase line of contact will probably lie along particle edges.

Displacement pressures in porous solids are often assumed proportional to the cosine of the contact angle. When an attempt is made to deduce contact angles from capillary displacement pressures, special attention must be given to the possible effect of edges (*29*). Even if the solid is smooth, capillary displacement pressure is proportional to the cosine of the contact angle only for extremely simple geometries such as uniform capillary tubes.

Although the solid edges may be important in determining configurational stability of the interface separating the two fluids, their contribution to surface free energy can be neglected; as with three-phase lines of contact at smooth solid surfaces, there are relatively

few molecules in the three-phase confluent zone compared with the total in all of the surface zones.

Contact angle hysteresis. Values of contact angles measured in real systems usually depend upon whether the three-phase line of contact is advancing or receding over the solid surface. Contact angle hysteresis can arise because of surface roughness, heterogeneous distribution of adsorbed impurities on the solid surface or the mechanism by which liquid molecules adsorb and desorb when the interface is displaced (*30*). If sufficient care is taken in preparation of a clean, smooth, solid surface, contact angle hysteresis can sometimes be reduced to less than one or two degrees (*31*).

Contact angles are clearly important in determining the capillary properties of porous media. However, in view of the difficulties of measuring reproducible contact angles on carefully prepared surfaces and the relaxed stability conditions at solid edges, it seems highly unlikely that all three-phase lines of contact within porous media will lie on smooth solid surfaces with a single-valued, uniform contact angle.

The present study is concerned with a quantitative treatment of displacement thermodynamics; hence, contact angle must be eliminated as an unknown variable since surface free energy is dependent on contact angle. Absence of contact angle hysteresis in experiments with porous media can only be confidently assumed when the liquid spreads over the solid. The contact angle is then zero if the three-phase line of contact lies on a smooth solid surface.

Surface energetics of spreading. In addition to disagreement on the general validity of Young's equation, there is also controversy as to its interpretation when the contact angle is zero (*7, 32*). Perhaps this is because Young's equation is commonly introduced by considering the balance of forces at the three-phase line of contact of a drop sitting on a plane solid surface. When the contact angle is zero, the drop will spread indefinitely. For the purpose of illustrating stability at plane surfaces, the above physical example is clearly inadequate.

A hypothetical model designed for general discussion of stability at plane interfaces was recently introduced by Melrose (*33*). The two fluids were a liquid, L and its vapor V. In this model, a plane liquid-vapor surface can coexist with a plane solid surface over which the liquid will spread. Spreading is prevented by a frictionless and inert mechanical barrier which can only move parallel to the solid surface. An essential requirement of the model is that the gravitational potential of the liquid be negligible. Only the main features of the model are depicted in Figure 3.

When the liquid is nonspreading, a force, Ω per unit length of the barrier, must be exerted to prevent contraction of the liquid surface. The force is given by

$$\Omega = \sigma_{lv} + \sigma_{sl} - \sigma_{sv} \tag{39}$$

From Young's equation 34 for finite contact angle, Ω is given by

$$\Omega = \sigma_{lv}(1 - \cos\theta) \tag{40}$$

On the other hand, for the spreading condition, adsorption of vapor will continue until the force, Ω, required to retain the barrier, vanishes. At this point, the system is asserted to be in equilibrium. For the nonspreading case, work is required to extend the liquid surface by moving the barrier; in the spreading system at equilibrium, however, the position of the barrier does not alter the free energy of the system since the barrier can be moved without expending work. In other words, if the adsorbed film is replaced by a thin liquid layer, there is no change in the surface free energy of the system.

Stability of the adsorbed film involves the limit of film thickness achieved at the expense of the liquid (*33*). Equilibrium requires that the outermost molecules of the film have the same chemical potential as the vapor and the surface molecules of the liquid. To attain this condition, the adsorbed film must thicken until its outermost molecules are unaffected by the attractive forces of the solid. Thus, the tension of the outermost part of the adsorbed film must be equal to that of the liquid-vapor surface. Similarly, the tension of the region of the film in contact with the solid is equal to the solid-liquid tension. Films of this nature were described by Harkins as duplex (*34*).

Spreading against Gravity. Figure 4a depicts spreading up a vertical infinite flat plate in a gravitational field with water and its vapor at equilibrium. If the vapor pressure at the level of the free water surface is p_o, the vapor pressure, p, at any height, h, above the plane water surface is given by

$$p = p_o \exp\left(-\frac{\Delta\rho g h M}{RT}\right) \tag{41}$$

where $\Delta\rho$ = density difference of liquid water and its vapor
g = acceleration due to gravity
M = molecular weight
R = universal gas constant

Vapor pressure is expressed in Figure 4a as percent relative humidity, H_R, where

$$H_R = \frac{p}{p_o} 100 \tag{42}$$

At an infinite height, the vapor pressure is zero and the tension is that of the solid against a vacuum denoted by σ_s. At finite heights, adsorption of vapor at the solid surface causes the thickness of the film to increase slowly with decreasing height as shown qualitatively in Figure 4a. The actual thickness of the adsorbed film and thickness variation with height are not known with any certainty; unpublished estimates for high relative humidities range from 10 to 30 Å (4 to 12 molecular layers of water) with 100 Å as an upper limit. There is mixed evidence that the solid can extend its range of influence on the structure of water to even greater distances but such considerations are beyond the scope of this paper (*35–37*).

Melrose (*33*) employs the relationship, due to Buff (*38*), between tension and stress distribution in an interface to illustrate qualitatively the formation of a duplex film when the vapor pressure over a plane solid is raised to its saturation value. Tension, σ, in the surface is given by

$$\sigma = \int (\mu_T - \mu_N)\, d\lambda \qquad (43)$$

where μ_T and μ_N are the transverse and normal components of the stress tensor in an interfacial region with integration over a normal, λ, to the interface.

Sketches of variation in stress anisotropy with vapor pressure given by Melrose (*33*) are included in Figure 4b to provide a rough, qualitative indication of how stress anisotropy in the surface varies with height. Although the presence of adsorbed material reduces the tension of the solid surface, the adsorbed water contributes to the total tension. As the film thickens, two maxima in stress anisotropy are conceived; at higher vapor pressures, the two contributions to tension become increasingly distinct (Figure 4b). If the plate touches the water surface, capillary rise against the plate to a maximum height of $\sqrt{2\sigma_{wv}/\Delta\rho g}$, precludes the existence of adsorbed vapor films below this height. At the water surface, the relative humidity is 100%, and a stable adsorbed film at this level would correspond to the duplex film given by the hypothetical model shown in Figure 3.

In this limiting case of film stability, the central minimum of the stress anisotropy diagram just touches the zero axis with separate surface-film and film-vapor regions contributing to the film's total tension. Further condensation of vapor would lead to the formation of a bulk liquid region separating liquid-solid and vapor-solid surfaces. The stress distribution in each of these surfaces is precisely that of the individual components of the duplex film; the stress distribution diagram for the system will now feature a central minimum of zero with finite length corresponding to the bulk water separating the solid-liquid and liquid-vapor surfaces.

In an adsorbed film, the distribution of mass in excess of the mass of displaced vapor is directly related to the variation of superficial tension with height. Gibbs (*39*) discusses the distribution of adsorbed material on a solid surface in a gravitational field. Young's equation is shown to follow from the special case of a local force balance at the three-phase line of contact that is equally valid for finite and zero contact angle. Gibbs discusses the variation in excess mass of the adsorbed material with height in terms of superficial tensions. At a particular height, h, the excess mass, m, of the adsorbed film is related to the superficial tension, η, by

$$d\eta = (mg)dh \qquad (44)$$

Thus, the excess mass, m', of adsorbed materials between any two given heights (h_1 and h_2, $h_1 < h_2$), is equal to the difference in superficial tensions at these heights.

$$m'g = (\eta)_{h2} - (\eta)_{h1} \qquad (45)$$

A more physically appealing statement of the above force balance is given directly by the increase in area under the stress anisotropy curves for the two given heights. The superficial tension is related to the stress anisotropy distribution by

$$\eta_h = [\int (\mu_T - \mu_N)\, d\lambda]_h - [\int (\mu_T - \mu_N)\, d\lambda]_{h=\infty} \qquad (46)$$

From Equations 45 and 46,

$$m'g = [\int (\mu_T - \mu_N)\, d\lambda]_{h2} - [\int (\mu_T - \mu_N)\, d\lambda]_{h1} \qquad (47)$$

Capillary Equilibrium in Gravitational Field. Bulk water can also exist at equilibrium above the free water surface if suitable solid boundaries are provided. As a simple illustration, capillary rise for zero contact angle in a 10-μ diameter tube is included in Figure 4a. The vapor above the curved water surface is in equilibrium with the adsorbed film at this height on the flat plate. The equilibrium capillary pressure of any vapor-water surface is fixed by its height above the free water surface.

$$P_c = \Delta\rho g h \qquad (48)$$

The capillary pressure is related to surface curvature by the Laplace equation (*40*)

$$P_c = \sigma_{wv}\left(\frac{1}{r_1} + \frac{1}{r_2}\right) \qquad (49)$$

where σ_{wv} is the water-vapor surface tension and r_1 and r_2 are the principal radii of curvature at any point in the surface, usually defined as positive with respect to the nonwetting phase. If the surface between water and its vapor is stable, Equations 48 and 49 apply for any shape of solid surface and any wettability condition.

Also depicted in Figure 4a are two sets of touching spheres at heights of 100 and 1000 cm above the free water surface. Water will condense around the points of contact between the spheres until the pressure drop across the surface of the pendular ring so formed corresponds to capillary pressure given by Equation 48. The properties of pendular rings are well documented (*41–44*). Profiles for pendular rings at equilibrium between 10-μ diameter hydrophilic spheres at the two heights are included in Figure 4a.

Properties of adsorbed films on curved solid surfaces, such as the tube and sphere surfaces shown in Figure 4a, will vary slightly from those on the plane surface at the same height. The thickness of adsorbed film on a curved solid surface will be about equivalent to that given by the plane surface at a height corresponding to the equilibrium curvature of the vapor-water surface increased by the curvature of the solid (taking convex as positive). Thus, at any height, adsorbed films are slightly thinner on convex solid surfaces and slightly thicker on concave solid surfaces than the equilibrium film thickness on the corresponding plane surface.

When spreading occurs, the surface free energy per unit area of adsorbed film will be equal to that of the vapor-liquid surface at the same height. For the range of capillary pressures and fluid curvatures of interest,

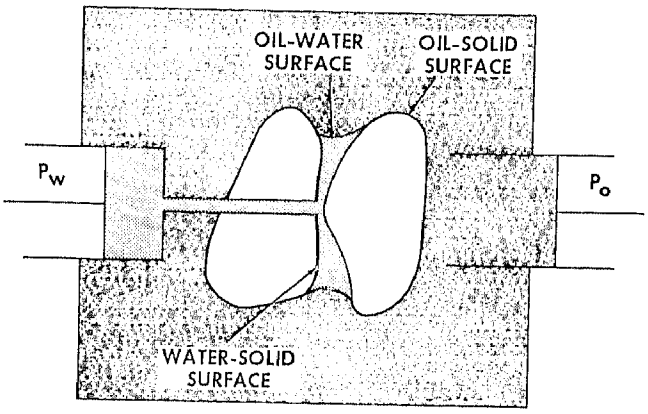

Figure 5. Idealized system for reversible immiscible displacement

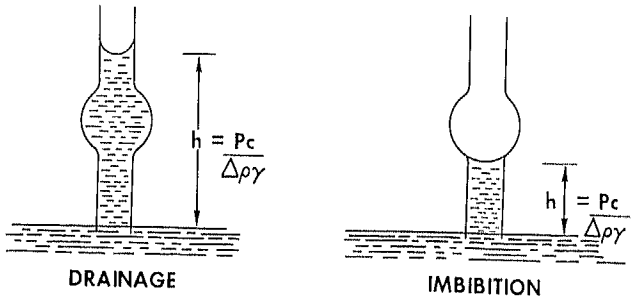

Figure 6. Bistability of an interface in a nonuniform tube

variation of vapor-liquid surface tensions with curvature are not measurable and can be neglected until the radii of curvature approach molecular dimensions (*15–17*). Also, for all practical purposes, the area of a surface is adequately defined by its physical position. Thus, for the spreading situation, the increase in free energy due to surface over the reference state given by solid overlain by bulk water is

$$\Delta F = \sigma_{wv}(A_{wv} + A_{sv}) \tag{50}$$

This result is often stated without formal derivation. The above discussion serves to demonstrate a fundamentally consistent treatment of surface energetics for spreading systems and clarifies the assumptions leading to Equation 50.

Thermodynamics of Reversible Displacement

The thermodynamics of reversible fluid displacement are now considered for an idealized model; changes of surface area within the model system are related to external work done on or by the system.

By the first law of thermodynamics, a change in the total energy of the system, dE, is given by

$$dE = dq + dW + \sum_{i=1}^{j} \mu_i dn_i \tag{51}$$

where dq is the heat flowing into the system. For an isothermal change

$$dq = TdS' \tag{52}$$

dW = the reversible work done on the system
μ_i = the chemical potential, and n_i is the number of moles of the ith component
j = the number of components

In the following analysis, gravitational, magnetic, and electric force fields are assumed to be absent or of negligible effect.

The work dW done on the system is given by

$$dW = -\sum_{p=1}^{3} P_p dV'_p + \sum_{k=1}^{3} \sigma_k dA_k \tag{53}$$

where p = the pth phase

and σ_k = interfacial tension of the kth surface
A_k = area of the kth surface
V' = volume

(We may note that two phases correspond to only one interface. In the above system, there are three phases and three interfaces. With four phases, six interfaces are possible, and so on.) If the system is closed,

$$dn_i = 0 \qquad i = 1, j \tag{54}$$

and

$$dE = TdS' - \sum_{1}^{3} P_p dV'_p + \sum_{1}^{3} \sigma_k A_k \tag{55}$$

The Helmholtz free energy is defined by,

$$F = E - TS' \tag{56}$$

$$dF = dE - TdS' - S'dT \tag{57}$$

Thus from Equations 55 and 57,

$$dF = -S'dT - \sum_{p=1}^{3} P_p dV'_p + \sum_{k=1}^{3} \sigma_k dA_k \tag{58}$$

If displacement is isothermal,

$$dF = -\sum_{p=1}^{3} P_p dV'_p + \sum_{k=1}^{3} \sigma_k dA_k \tag{59}$$

To facilitate discussion, we will assume a model system consisting of a solid(s), wetted by water (w) with a unique contact angle θ, in the presence of oil (o). Figure 5 depicts a pendular ring of water held between two solid particles. The water can enter or leave the ring *via* a passage through one of the particles. The geometry of the particles allows the ring to vary smoothly and reversibly in volume and surface area. The walls of the piston are assumed to make no contribution to the surface free energy.

If the pistons were free to move, water would tend to be imbibed and the pendular ring would grow. If the piston in contact with the oil is free to move, an outward force proportional to $(P_o - P_w)$ must be exerted on the piston in contact with water in order to maintain equilibrium. The external work, W_{ext}, done on the enclosed system in moving the piston in contact with the water outward to give a displacement, $-dV_w$, where V_w is the volume of water in the pendular ring, is given by:

$$dW_{ext} = -(P_o - P_w)dV_w \tag{60}$$

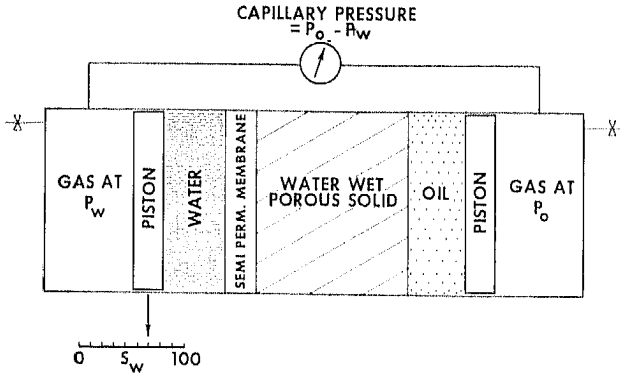

Figure 7. Idealized capillary pressure apparatus

The decrease in Helmholtz free energy of the surroundings of the closed system is equal but opposite in sign to the work done on the closed system. From Equation 59 the change in Helmholtz free energy, dF, of the closed system can be written

$$dF = -P_s dV'_s - P_w dV'_w - P_o dV'_o + \sigma_{wo} dA_{wo} + \sigma_{so} dA_{so} + \sigma_{sw} dA_{sw} \quad (61)$$

For a virtual displacement, the total change in the Helmholtz free energy of the system and its surroundings is zero.

$$dF_{tot} = 0 = (P_o - P_w) dV_w - P_s dV'_s - P_w dV'_w - P_o dV'_o + \sigma_{wo} dA_{wo} + \sigma_{so} dA_{so} + \sigma_{sw} dA_{sw} \quad (62)$$

If the work on compression on all three phases is neglected,

$$dV'_s = dV'_w = dV'_o = 0 \quad (63)$$

Also, the total solid surface area is constant so that,

$$dA_{so} = -dA_{sw} \quad (64)$$

and from Young's equation (see Equation 34)

$$\sigma_{so} - \sigma_{sw} = \sigma_{wo} \cos \theta \quad (65)$$

The pressure difference $(P_o - P_w)$ is the capillary pressure P_c across the curved water-oil interface.

Equation 62 can therefore be reduced to

$$-\int P_c dV_w = \sigma_{wo} d(A_{wo} + A_{so} \cos \theta) \quad (66)$$

If the water spreads over the solid, $\cos \theta = 1$, and

$$dF = -\int P_c dV_w = \sigma_{wo} d(A_{wo} + A_{so}) \quad (67)$$

For finite displacements which can be conducted reversibly Equations 66 and 67 can be integrated to give, respectively

$$\Delta F = -\int_{v_1}^{v_2} P_c dV_w = \sigma_{wo} (\Delta A_{wo} + \Delta A_{so} \cos \theta) \quad (68)$$

and

$$\Delta F = \int_{v_1}^{v_2} P_c dV_w = \sigma_{wo} (\Delta A_{wo} + \Delta A_{so}) \quad (69)$$

The above thermodynamic analysis of reversible displacements will next be extended to a treatment of displacement in porous media.

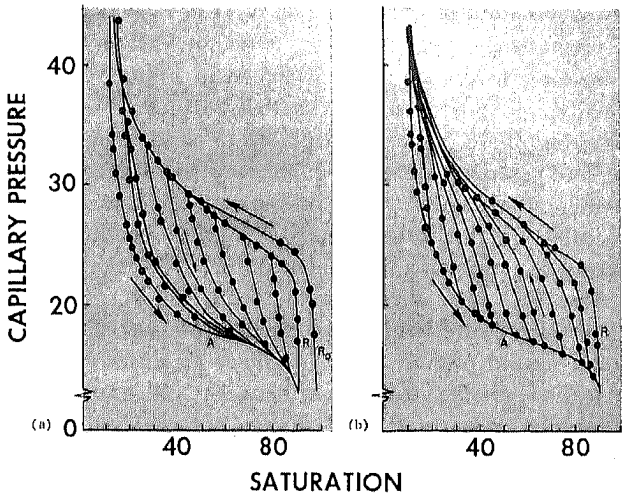

Figure 8. Capillary pressure hysteresis data for 48–60 mesh microbeads (64)

THERMODYNAMICS OF IMMISCIBLE DISPLACEMENT IN POROUS MEDIA

Relationships between capillary pressure and displacement volume can be obtained by a number of routine procedures which are adequately described elsewhere (*45–48*). Equations 68 and 69 have often been applied directly to determine changes in surface area (*47–54*); this necessarily assumes that displacement can be conducted smoothly and reversibly. The assumption of reversible displacement is at variance with commonly observed hysteresis in capillary pressure. Irreversibility at the microscopic scale is evident from observations made by Haines (*2*); during invasion of pore spaces, the development of unstable interface configurations caused small oscillations in pressure. Striking demonstrations of the discontinuities in capillary pressure *vs.* displaced volume were reported recently by Crawford and Hoover (*55*).

The bistability of an interface in a nonuniform capillary of the type shown in Figure 6 is commonly used to explain capillary pressure hysteresis. Liquid level depends upon its initial condition. Furthermore, when the filled tube is slowly raised above the free water surface, the interface passes into the bulbous region spontaneously unless restrained by carefully controlling the pressure in the tube above the interface. Similarly, when the drained tube is slowly lowered, the liquid will imbibe spontaneously into the bulb, but at a pressure distinctly different from the drainage pressure.

It follows that when given volumes of fluid are comingled in a complicated network of nonuniform pores typical of a porous media, many stable fluid configurations are possible. Unlike many thermodynamic systems which are stable at a single minimum free energy, there will be many local minima of free energy, and the global minimum for the system has no special significance.

Measurement of Capillary Pressures in Porous Solids

An idealized apparatus for measurement of capillary pressures in porous solids is shown in Figure 7. Normally, the porous solid is initially saturated with the wetting phase (water) and placed in close contact with a fine-pored membrane which remains saturated with water at all times. The pressure on the water phase (neglecting hydrostatic head) is the measured gas pressure acting on a frictionless piston. The nonwetting phase (oil) is in direct contact with the porous solid, and its pressure is given by the gas pressure P_o acting on a second piston. Since capillary pressure is defined as the pressure difference between oil and water, absolute pressures P_o and P_w are not required. Normally, one phase or the other is at atmospheric pressure throughout the measurements.

Displacement in the porous solid is usually expressed as per cent change in saturation, S_w, the volumetric fraction of pore space in the solid occupied by the wetting phase. Displacement of a volume of water ΔV_w is related to a saturation change ΔS_w by

$$\Delta V_w = V_B \phi \Delta S_w \qquad (70)$$

where V_B is the bulk volume of the porous solid and ϕ is the porosity of the solid. Changes in saturation result from changes in pressure. Each capillary pressure data point is obtained by holding the external pressure difference at a constant value until fluid flow to or from the porous solid ceases. In the apparatus of Figure 7, volumetric displacement and the time at which flow ceases is indicated by the position of the piston acting on the water phase.

Data points are usually referred to as capillary pressure equilibria; but this description requires qualification because not all of the stability requirements for equilibrium are met. Before discussing the nature of the stability represented by capillary pressure data points, the general form of capillary pressure *vs.* saturation curves will be reviewed.

General form of capillary pressure data. Saturation changes which result from variations in capillary pressure do not follow a unique functional relationship. Plots of capillary pressure data *vs.* saturation are shown in Figure 8a and b. To aid discussion of capillary pressure curves, we define the following terms.

- Irreducible saturation, S_{wi}: the volume of wetting phase retained at high capillary pressures where the wetting phase saturation appears to be independent of further increases in the externally measured capillary pressure.
- Residual saturation, S_{or}: the volume of nonwetting phase which is entrapped when the externally measured capillary pressure is reduced from a high value to zero (see Figure 8a).
- Initial drainage curve, R_o: the relationship characteristic of displacement of wetting phase from 100% saturation to the irreducible wetting phase saturation, S_{wi}.
- Imbibition, A: increase in wetting phase saturation from the irreducible wetting phase saturation to the residual nonwetting phase saturation, S_{or}.
- Secondary drainage, R: drainage from the residual nonwetting phase saturation, S_{ro}, to the irreducible wetting phase saturation, S_{wi}.

Most experimental evidence indicates that the irreducible saturation obtained by initial drainage is the same as that obtained by secondary drainage. When the two conditions are the same, imbibition after secondary drainage will follow exactly the imbibition curve obtained after initial drainage. Thus, the secondary drainage curve and the imbibition curve constitute a closed and reproducible hysteresis loop, RA.

Scanning curves within the main hysteresis loop, RA, are obtained by reversing the direction of pressure change at some intermediate point along the secondary drainage or imbibition curves. In the former case, they will be called primary imbibition scanning curves, and in the latter, primary drainage scanning curves.

Hysteresis. Many natural systems exhibit hysteresis in the relationship of one variable to another. Sometimes hysteresis, as judged by the magnitude of the hysteresis loop, can be reduced merely by increasing the time for traversal of a loop. If the loop degenerates into a line, then hysteresis is clearly time-dependent. Capillary pressure hysteresis in porous media is essentially independent of time in that the loop cannot be reduced by further increasing the experimental time for each data point. Such behavior has been named permanent hysteresis (*57*).

Everett and coworkers (*56–59*) developed an independent domain theory of permanent hysteresis which has recently been investigated as a model for capillary pressure hysteresis (*60–62*). Everett's theorems can be stated for experimentally observed capillary pressure behavior as follows:

1. The secondary drainage curve, R, and the imbibition curve, A, form a closed loop, RA, with all subsequent capillary pressure data points lying on or within this loop (Figures 8a and b).
2. The primary drainage scanning curves, which begin at the imbibition curve, A, either meet at the upper intersection of the RA curve (Figure 8b), or

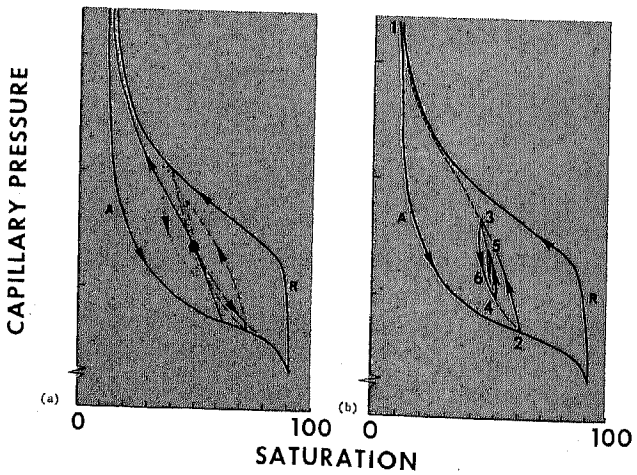

Figure 9. General behavior of capillary pressure scanning curves

Table II. Comparative Reductions in Relative Humidity of Water Due to Surface Curvature, Temperature Reduction, and Salinity

Capillary pressure, h, cm H_2O ($P_c/\Delta\rho g$)	Surface curvature, cm^{-1} (P_c/σ_{wv})	Cylindrical capillary radius, ($\theta = 0$), cm ($2\sigma_{wv}/P_c$)	Percent relative humidity, 20°C, (p/p_0) 100%	Equivalent temperature reduction ΔT below 20°C	Equivalent salinity, (gmol NaCl per liter)
0	0	∞	100	0	0
10	1.36×10^{2}	1.47×10^{-2}	99.999	1.6×10^{-4}	3×10^{-4}
10^{2}	1.36×10^{3}	1.47×10^{-3}	99.99	1.6×10^{-3}	3×10^{-3}
10^{3}	1.36×10^{4}	1.47×10^{-4}	99.92	1.3×10^{-2}	2.4×10^{-2}
10^{4}	1.36×10^{5}	1.47×10^{-5}	99.27	1.2×10^{-1}	0.22
10^{5}	1.36×10^{6}	1.47×10^{-6}	93.0	1.16	2.1

converge tangentially onto the secondary drainage curve, R, in a region close to the intersection. Behavior of imbibition scanning curves, which begin at the drainage curve, R, is analogous (Figure 8a).

3. Any point within a hysteresis loop can be reached by many paths. Complete specification of the system at a given pressure-saturation coordinate must include the path by which the point was attained, since the path determines the microscopic distribution of the fluids and future behavior of the system. (Four possible paths to the same pressure coordinate are shown in Figure 9a.)

4. If the system were taken through a series of pressure oscillations of decreasing amplitude, after the nth pressure reversal, the system moves toward the point at which the $n - 1$ reversal occurred, and if the system is carried through this point, it moves toward the $n - 3$ reversal point, and so on. (This behavior is shown in Figure 9b.)

The above theorems describing the general behavior of capillary pressure curves are consistent with the expected displacement mechanism. Closed scanning loops can be explained as follows. Consider a region which has been drained to a saturation S_{w1} by a pressure P_1. If the pressure were then lowered to P_2, the wetting phase would imbibe to S_{w2}. When the pressure is raised again to P_1, precisely that region which became occupied by imbibition (when the pressure was lowered from P_1 to P_2), can be expected to drain. The liquid in this region must have continuity because it imbibed; the previous drainage demonstrated that reapplication of pressure P_1 will be sufficient to remove only that liquid from the region where liquid was freshly imbibed. Equally straightforward, but not entirely rigorous, explanations can be given for the other general statements made above.

For a porous medium to satisfy the conditions of Everett's independent domain model, each pore must have a characteristic drainage pressure p_1 and a filling pressure p_2. The model does not require that p_1 and p_2 be functionally related. If the conditions of the independent domain theory hold for porous media, then imbibition scanning curves could be used to predict drainage scanning curves and *vice versa*. Satisfactory predictions were obtained by Poulovassilis (*60*) in tests on beds of sintered glass beads; however, later work by Topp and Miller (*62*) showed that the theory is not generally applicable.

In general, assignment of draining and filling pressures to a given region may be unrealistic, since pressures for displacement are also determined by accessibility and phase continuity. When the behavior of a domain is influenced by other domains, the system is said to exhibit cooperative behavior. In other words, the behavior of any given pore depends on its neighbors. A model of hysteresis which includes cooperative behavior has been investigated by Enderby (*63*).

Another fundamental weakness in applying the independent domain theory to displacements in porous media is that pore space cannot be divided precisely into volumetric zones which exhibit one to one correspondence with respect to drainage and imbibition behavior. Although capillary behavior is commonly discussed in terms of pores, no definition of the bounds of a single pore exists for real porous media. If a definition were attempted in terms of capillary behavior, a first requirement would be that a distinction should be made between imbibition and drainage conditions.

Stability of capillary pressure points. When two homogeneous fluid phases are held within a porous solid, a necessary condition for equilibrium, neglecting gravity, is that capillary pressure across the interface separating the two fluids be the same everywhere. The form of capillary pressure curves indicates that this condition is not satisfied at each point. For example, when water is displaced by oil, some water becomes trapped in small pores and around points of contact between particles. Once hydraulic communication *via* bulk water paths is lost, volumes of water elements cannot adjust quickly to attain equilibrium with the externally measured pressure. As drainage progresses, increasing amounts of wetting phase are isolated and an irreducible wetting phase saturation is reached (*2*, *47*). At this stage only continuous oil and hydraulically discontinuous water are retained. Hence, the externally measured capillary pressure bears no relationship to the capillary pressures of oil-water interfaces within the porous medium. Similarly, during imbibi-

tion, the oil phase is not completely displaced. When the external capillary pressure is reduced to zero, globules of residual oil are retained at pressures higher than the water which surrounds them. Both trapped oil and trapped water will tend to diffuse within the porous solid; however, the time required to reach equilibrium by diffusion is long and experimentally prohibitive.

Although discontinuous elements are not at equilibrium, capillary pressure data points can be regarded as stable if we assume that changes in their volume can be neglected for the duration of an experiment. Experimental data points can then be assumed to correspond to an idealized model, with no mass transfer across phase boundaries or *via* films retained at the surfaces of drained solids (*64*). Under these conditions, only those interfaces which can adjust curvature by hydraulic flow of both fluids maintain capillary equilibrium with the externally measured capillary pressure; elements of fluid at differing pressures can coexist indefinitely until the region they occupy is encroached upon by an invading continuous region of the same phase.

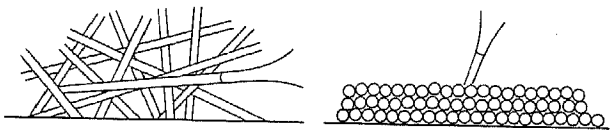

Figure 10. Experiments illustrating fluctuations in pressure during drying

The above model appears to hold well for so-called clean solids. When the solid surface of a porous system is rough and channeled, or has a coating of colloidal particles, hydraulic conductivity may never be lost completely. The almost isolated wetting liquid may approach equilibrium at much faster rates than in a comparable situation with smooth surfaces; this could even permit stability to be achieved through attainment of a true capillary equilibrium. (There is no violation of the model in these cases because the almost discontinuous liquid is still strictly classified as continuous.) In general, the applicability of the above capillary behavior model must be judged by examining the stability of experimental capillary pressure data points. Another indication of applicability is the development of an irreducible saturation which is distinctly independent of both time and further increases of the external capillary pressure.

Stability can also be affected by temperature. Sometimes it is claimed that a true capillary equilibrium would be obtained if capillary pressure experiments were conducted over sufficiently long times. For example, if a column of particles were drained of water with air as the nonwetting phase, the observed and apparently stable distribution of water would slowly change by diffusion (caused by differences in vapor pressure due to curvature) until a true capillary equilibrium is reached (*65*). Aside from the long time required for diffusion, the need for adequate temperature control would make such an experiment difficult to execute. The temperature reduction necessary to lower the vapor pressure by the same amount as that due to surface curvature alone is given in Table II (*66*). Vapor pressure is extremely sensitive to temperature. Thus, changes due to diffusion that are observed over long time periods are probably caused by ambient temperature variations. It follows that accurate temperature control is needed for capillary pressure experiments that take several days or even months to complete even though the measurement of true capillary pressure equilibria is not the objective.

Vapor pressure of water is also sensitive to salt concentration. Salt concentration (gmol of sodium chloride/l.), necessary to reduce the vapor pressure by an amount equivalent to effects of surface curvature alone, is also listed in Table II. Vapor pressure above a curved surface of a salt solution depends on both curvature and concentration; thus liquid volumes at different capillary pressures and salinities could exert equal vapor pressures and be in stable equilibrium with each other. For isolated volumes of water, each of which contains a fixed weight of salt, any variation in volume will result in a change in salt concentration which will tend to stabilize the volume variations. Thus, if saline water were used in capillary pressure experiments, applicability of the idealized model of capillary behavior would be enhanced.

Haines Jumps

The basis for treating experimental capillary pressure points as stable has now been established. We will now consider the behavior of the system during displacement. A basic feature of fluid interface motion during displacement is the Haines jump resulting from unstable fluid configurations (*2*, *67*, *68*). These jumps are illustrated by the following simple experiments.

In the first experiment, melting point tubes were heated and pulled into long fine capillaries which were broken into short lengths. These tube segments were then piled in a heap, saturated with a volatile liquid, and the system was observed through a microscope as the wetting-phase saturation decreased by evaporation (Figure 10a). The tubes were slightly tapered and the air-liquid menisci moved slowly toward the narrower ends of the tubes as the saturation decreased and the capillary pressure increased. Occasionally, a meniscus would suddenly recede or jump back toward the wider ends, indicating a sudden pressure change. The meniscus would then continue to displace smoothly from its new position until it suddenly kicked back again, and so on. In effect, each tapered tube served as a pressure measuring device which showed that capillary pressure does not rise smoothly and continuously with decrease in saturation.

In a second experiment on packings of 3 mm spheres, sudden flexures in the interface as described by Haines again indicated that pressure was not increasing mono-

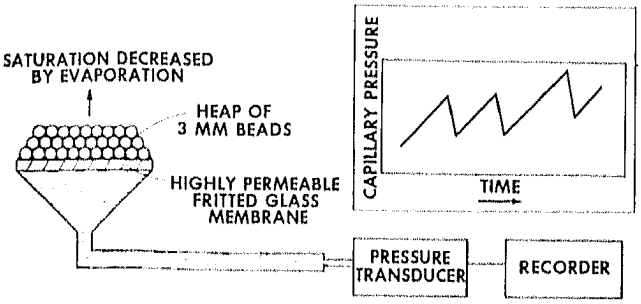

Figure 11. Apparatus for recording pressure fluctuations

tonically with saturation. When the tapered end of a melting point capillary was inserted into the pile of spheres (Figure 10b), the liquid in the tube behaved erratically as it followed pressure changes in the bead pack.

The same spheres were heaped on a highly permeable fritted glass membrane connected with a sensitive pressure transducer as depicted in Figure 11. The bead pile was saturated with volatile liquid. As the liquid evaporated, the recorded variation of pressure with time was of the form shown in Figure 11. The pressure rose relatively slowly, and then suddenly fell, then slowly rose again, and so on.

The above experiments clearly demonstrate that displacement cannot be conducted smoothly and reversibly because of spontaneous changes in fluid configuration. In the next section a new treatment of displacement as a distinctly quantized process is developed from application of thermodynamic fundamentals.

Infinitesimally Slow Displacement

First we consider infinitesimally slow withdrawal of liquid from the capillary model shown in Figure 12. Liquid can be removed reversibly from both tubes of the model until the meniscus in the tube on the right meets the enlargement in tube cross section at *A*. Boundary conditions at *A* cause the interface to become unstable, and the liquid descends rapidly through the upper bulb to a stable position in the vicinity of *B*. If the hole through which fluid is withdrawn were infinitesimally small, we would have the limiting case of no liquid flow during the spontaneous motion of the interface. Alternatively, we could envision use of an idealized valve which would only permit flow if the pressure drop across it were infinitesimally small.

If a finite pressure developed across the valve because of an unstable fluid configuration, the valve would close instantly; the valve would reopen only after the fluid had attained a stable configuration, and the fluid pressure on the outlet side of the valve was adjusted to equal the system pressure. From this point, further removal of fluid could be effected under reversible conditions until the system again becomes unstable as the lower bulb drains spontaneously.

Again, a spontaneous redistribution of fluid results in a reduction of capillary pressure. If capillary pressure were plotted against volume of liquid in the model, we would see that displacement under these idealized circumstances consists of smooth, reversible changes linked by spontaneous changes in pressure at constant saturations. The sequence of alternate reversible and irreversible changes during this quantized displacement would be determined by the detailed structure of the model.

The above argument can be extended in principle to the complicated structures of porous media. Instability can be regarded as localized to a single pore or a group of pores. The capacity of the rest of the system to receive or give up a small volume of fluid, represented by the tube on the left in Figure 12, determines the size of the finite pressure change caused by the instability.

Rheons and Isons

The form of the pressure-volume relationship characteristic of the above model is similar to that obtained experimentally for the heap of 3-mm glass beads. In both cases, the pressure slowly increases as drainage progresses until an unstable fluid configuration precipitates a rapid pressure change. Reducing the drainage rate causes the sudden pressure changes to occur at almost constant saturation as in the model of Figure 12.

The sudden motions of unstable interfaces reflected by small changes in pressure have been described as Haines jumps or jerks (*67*, *68*). Heller (*69*) mentions that the term rheon has been suggested by J. C. Melrose as an alternative name for the Haines jump. In this treatment, we adopt the term *rheon* for a Haines jump which takes place at constant saturation. Under this condition, no external work can be done on or by the system during a Haines jump. The segments of the pressure–volume displacement curve between rheons correspond to smoothly reversible displacements; they will be called *isons*.

When capillary pressures are measured in fine-pored media, the discontinuities in pressure are generally too small to observe, and experimental capillary pressure curves, although not reversible, appear to be smooth and continuous. In theory, displacements from porous media could be conducted as described above for the tube model to give capillary pressure curves consisting

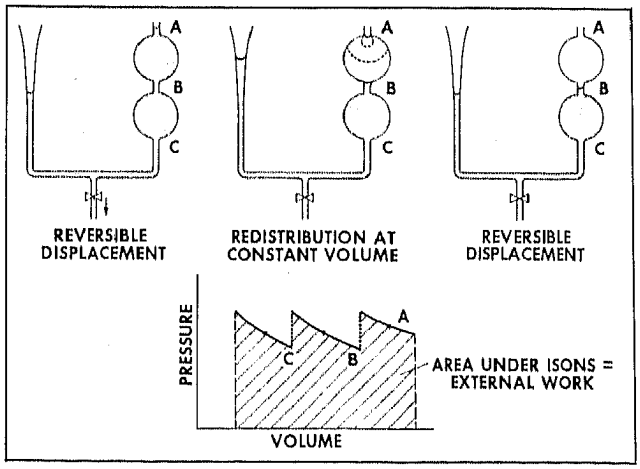

Figure 12. Infinitesimally slow drainage of a model capillary system

of series of isons and rheons. Since capillary pressure hysteresis is permanent with respect to time, we postulate that the experimental data give the same path, apart from loss of detail, as that which would be given by the isons and rheons. Thermodynamic relationships which apply to individual isons and rheons provide the basis for thermodynamic relationships which apply to experimental capillary pressure data.

Rheons. A rheon is defined as a spontaneous redistribution of fluid within a porous medium. Instabilities arise from fluid interfaces that are unable to change curvature smoothly with variations in pressure. The extent to which an interface can vary its curvature without spontaneous motion depends upon the boundary conditions at the surface of the porous solid. A general discussion of the stability of interfaces is given by Gibbs (*70*).

Once an unstable configuration is reached, the interface moves rapidly to a new equilibrium position. The volume of liquid spontaneously displaced from a region may vary from a fraction of a single pore space to an assembly of pores. For example, with rough surfaces, displacement from regions of a single pore could be likened to a ratchet mechanism. On the other hand, cooperative effects could cause displacement in large groups of pores during a single rheon. In general, the number of rheons contained by a capillary pressure *vs.* saturation curve can be expected to increase directly with sample size and be inversely proportional to the cube of the average pore diameter.

The magnitude of the finite pressure change accompanying a rheon depends on both the size of the region spontaneously vacated by a given fluid and the capacity of the system to advance its phase boundaries elsewhere. Generally in fine-pored solids the system capacity is large compared to the net volume of fluid redistributed by a rheon; hence, the pressure change is very small. The sign of the small changes in capillary pressure will be negative for rheons on drainage curves and positive for rheons on imbibition curves.

From the second law of thermodynamics the free energy of the system must be diminished as a result of the spontaneous change. Since the change occurs at constant saturation, no external work is done on or by the system and loss in free energy, ΔF, is given by

$$\Delta F = \sigma_{ow}(\Delta A_{ow} + \Delta A_{so} \cos \theta) \qquad (71)$$

where the quantity $(\Delta A_{ow} + \Delta A_{so} \cos \theta)$ must be negative. This loss of free energy is the most important characteristic of the rheon. As the pressure change associated with the rheon approaches zero, the decrease in surface free energy has a definite value.

Total surface energy including both surface free energy and surface heat of formation will finally appear as heat. For water against air, surface free energy at 15°C is approximately 74 ergs/cm² and heat of formation about 43 ergs/cm², giving a total energy of 117 ergs/cm². In general, the heat capacity of the system will be so large that the temperature changes accompanying loss of surface energy will be miniscule. Recovery of work because of the temperature difference of the system and its surroundings is not a serious possibility; we assume that the heat escapes until thermal equilibrium is established.

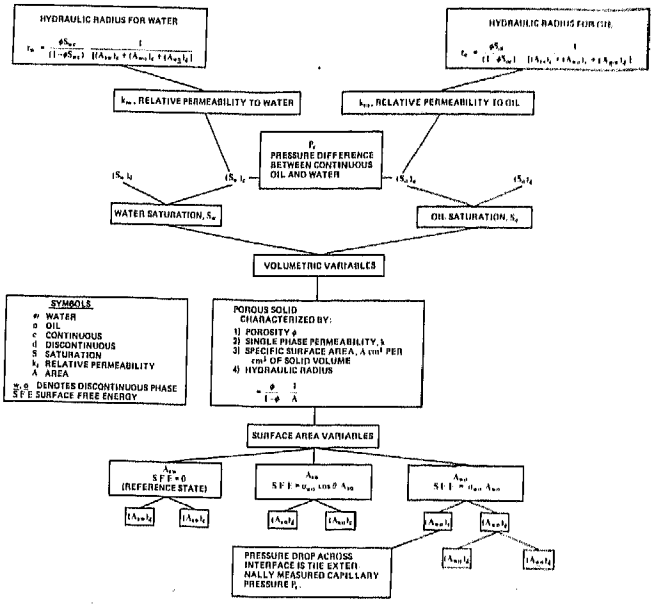

Figure 13. Relationships between volumetric and surface variables of two fluid phases in a porous solid

Isons. Isons are defined as displacements of one phase by another from porous media under balanced, stable conditions. These displacements are smooth and reversible with continuous variation of pressure with saturation. An ison's domain of stability with respect to saturation change extends in both directions from the saturation of the previous rheon; but the defined saturation range of an ison begins with its initial saturation and is terminated by the next rheon. Since isons and rheons occur alternately, the number of isons in a particular capillary pressure-saturation curve is governed by the same factors that determine the number of rheons.

For each individual ison the thermodynamic relationships developed for reversible displacements hold. Thus, under the conditions for which Equation 68 was derived, we have with Equation 70

$$\phi V_B \int_{S_{w1}}^{S_{w2}} P_c dS_w = \int \sigma_{wo} d(A_{wo} + A_{so} \cos \theta) \qquad (72)$$

where S_{w1} and S_{w2} lie within the domain of a single ison. For drainage, work is done on the porous system and the surface free energy of the system is increased; for imbibition, the system does work on the surroundings and surface free energy decreases. Changes are conducted isothermally with heat of surface formation continuously given up to or adsorbed from the surroundings.

Displacement Mechanism in Porous Media

A consistent account of the mechanism of displacement in porous media can be formulated within the framework of the quantized model. Interrelated changes

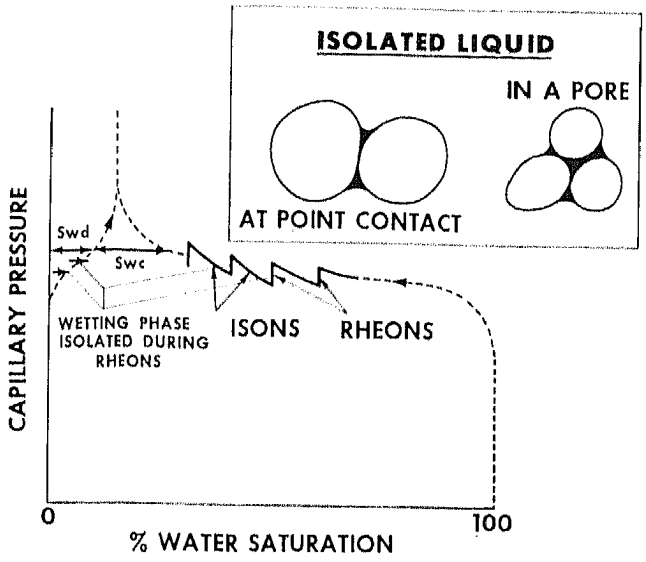

Figure 14. Detailed mechanism of drainage, showing isons and rheons of drainage curve and isolation of wetting phase

in the volumetric and surface area variables that occur during displacement are shown as dimensionless quantities in Figure 13. Volumetric variables are wetting phase (say water) saturation S_w, and nonwetting phase (say oil) saturation S_o. Portions of the volumes making up these saturations may have hydraulic continuity with the surroundings; other portions may not. The continuous and discontinuous portions are denoted by $S_{w,c}$ and $S_{w,d}$ respectively for water, and $S_{o,c}$ and $S_{o,d}$ respectively for oil. Surface area variables are the water-solid, oil-solid, and water-oil interfaces which bound the above volumes; these variables are expressed as fractions of the total solid surface area, A, and denoted by A_{sw}, A_{so} and A_{wo}, respectively. Each of these three surface areas can be subdivided into contributions from the continuous and discontinuous parts of each phase, denoted by suffixes c and d, to give six surface area variables in all: $(A_{sw})_c$, $(A_{sw})_d$, $(A_{so})_c$, $(A_{so})_d$, $(A_{wo})_c$, and $(A_{wo})_d$. The discontinuous oil-water interface area, $(A_{wo})_d$ can be further subdivided into $(A_{\underline{wo}})_d$ and $(A_{w\underline{o}})_d$ where the discontinuous phases are water and oil respectively (Figure 13). (Other quantities included in Figure 13 relating to relative permeability will be discussed in a later section of this paper.)

Variations of the above volumetric and surface quantities with respect to rheons and isons will first be considered for the initial drainage capillary pressure curve. For this curve, the porous solid is initially saturated with water and quantities $S_{o,d}$, $(A_{\underline{wo}})_d$, and $(A_{so})_d$ are always zero.

As drainage from 100% saturation progresses, some water is cut off by the invading oil and is retained around particle contacts and in the smaller pores as sketched in Figure 14. The manner in which the components S_{wc} and S_{wd} of the water saturation vary as drainage progresses is indicated by the wetting phase isolation curve of Figure 14. As the water saturation S_w decreases, the fraction of water which is discontinuous, S_{wd}, increases from zero until at the irreducible saturation S_{wi}, all of the retained wetting phase is held as disconnected volumes. With the disappearance of the continuous interface, $(A_{wo})_c$, the externally measured capillary pressure loses significance with respect to conditions within the porous solid.

The capillary pressure of an individual element of water will be approximately equal to the capillary pressure, P_c, across the continuous interface, $(A_{wo})_c$, at the time the element became isolated (*64*, *71*). This correspondence cannot be exact, however, because an element of wetting phase loses continuity by an irreversible rupturing process. Since irreversible changes are restricted to rheons, formation of a discontinuous element of liquid can only occur during a rheon. A rheon also occurs at constant saturation, S_w; thus, any increase in the discontinuous water saturation, ΔS_{wd}, must be exactly equal to the decrease in continuous water saturation, ΔS_{wc}. These exchanges must be finite

Table III. Relationships between Continuous and Discontinuous Fluid Saturations, Surface Free Energy and Work of Displacement for Isons and Rheons

	Drainage	Imbibition
Ison, (smoothly reversible displacement)	S_{wd}, S_{od}, $(A_{wo})_d$, $(A_{so})_d$, $(A_{sw})_d$ are constant $\Delta W = V_B\phi \int P_c dS_w$	
	$dS_o = [dS_w]$ $\Delta F = V_B\phi \int P_c[dS_w]$ $= \int \sigma_{wo} d\{(A_{wo})_c + (A_{so})_c \cos\theta\}$	$dS_w = [dS_o]$ $[\Delta F] = V_B\phi \int P_c dS_w$ $= \int \sigma_{wo}[d\{(A_{wo})_c + (A_{so})_c \cos\theta\}]$
Rheon, (spontaneous change at constant saturation)	S_o, S_w are constant $\Delta W = 0 \quad \Delta F < 0$ $[\Delta F] = [\Delta A_{wo} + \Delta A_{so} \cos\theta]$	
	$\Delta S_{wd} = [\Delta S_{wc}]$ $\Delta S_{oc} = [\Delta S_{od}]$	$\Delta S_{wc} = [\Delta S_{wd}]$ $\Delta S_{od} = [\Delta S_{oc}]$

Quantities in square brackets [ ] are negative unless equal to zero.

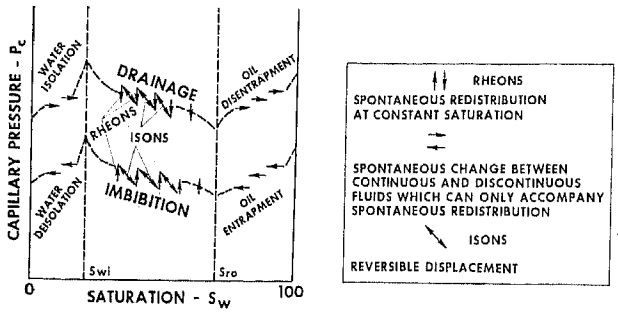

Figure 15. Detailed mechanism of displacement showing relationships between continuous and discontinuous parts of each phase during a drainage-imbibition cycle

and any number of discrete volumes of water could be isolated during a single rheon.

When water is imbibed, the fraction of discontinuous water decreases and we can postulate the existence of a water de-isolation curve which complements the measured capillary pressure imbibition curve. As with isolation of water during drainage, any union of the invading water with a discontinuous element of water will be irreversible and must be associated with a rheon. Some imbibition rheons may also include entrapment of oil as globules. Entrapment of oil tends to occur at relatively high water saturation (*72*). A capillary imbibition curve is depicted as a series of isons and rheons in Figure 15, together with water de-isolation and oil entrapment curves. Changes in the discontinuous saturations are shown as discrete steps. For simplicity we assume that no water remains trapped within regions occupied by the discontinuous oil.

Secondary drainage from the residual oil saturation S_{or} is similar to the initial drainage curve except that rheons may include both disentrapment of oil globules and isolation of water. The secondary drainage curve together with water isolation and oil disentrapment curves are also depicted in Figure 15. In all, Figure 15 includes three hysteresis loops. The central loop is the capillary pressure hysteresis loop which can be measured experimentally. In fine detail, these curves consist of isons and rheons as shown. The curves illustrating variations of discontinuous saturations (horizontal arrows) represent finite saturation changes with capillary pressure coordinates defined by the capillary pressure P_c measured at the time of formation or elimination of discontinuous elements.

The relationships between the surface area and volume quantities shown in Figure 13 for drainage and imbibition isons and rheons are summarized in Table III.

Free Energy Changes of Displacement

The area under a series of isons is exactly equal to the external work done on or by the system during displacement. Neglecting loss of fine detail in experimental capillary pressure data, the area under the isons also corresponds exactly to the area under a capillary pressure curve. This observation provides a consistent thermodynamic basis for the common assumption that the area under a capillary pressure curve corresponds to reversible external work.

The quantum approach is also useful in setting definite limits on surface free energy changes that accompany displacement. If a closed capillary pressure hysteresis loop is measured from wetting phase volume V_1 to a smaller volume V_2, the difference in surface free energy, ΔF, of the states corresponding to V_1 and V_2, lies between the work done on the system for drainage and the work recovered from the system for imbibition.

$$\int_{V_1}^{V_2} P_c dV > \Delta F > \int_{V_2}^{V_1} P_c dV \qquad (73)$$

(Pearce and Donald (*73*) attempt to define free energy changes more closely by comparing different work paths to the same pressure-saturation coordinate on the main hysteresis loop. Primary scanning curves are shown as closed loops which span intermediate points on a main drainage-imbibition loop. However, such behavior is not in accord with the general form of experimental capillary pressure hysteresis data.)

The area of the hysteresis loop is the minimum possible amount of work lost in describing the hysteresis loop. The area of the loop also gives the maximum error which arises from the often made assumption that work given by the area under a capillary pressure curve equals the change in surface free energy.

Any displacement represented by a capillary pressure curve will have a characteristic efficiency which is determined by the geometry of the solid. For example, the efficiency of initial drainage is given by the ratio of the increase in surface free energy of the system to the work of drainage.

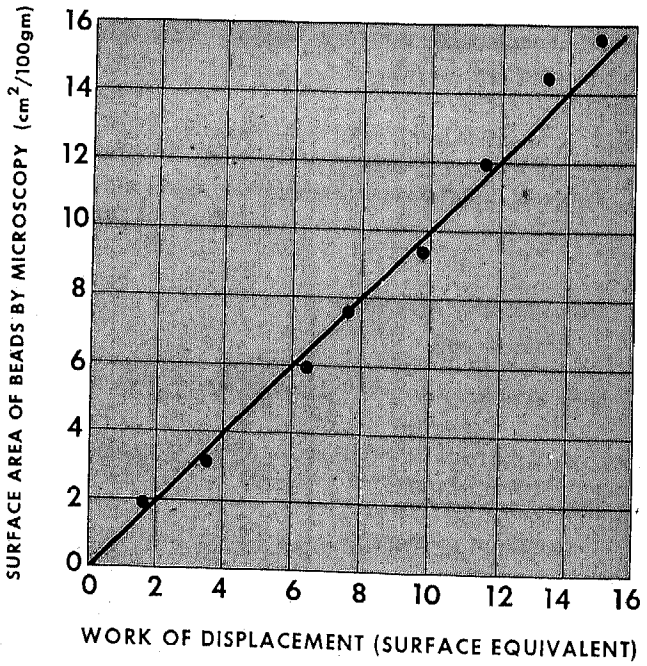

Figure 16. Solid surface area versus work of immiscible displacement for random packings of glass beads

Table IV. Surface Areas at Irreducible Wetting-Phase Saturation as Percent of Total Solid Surface Area from Analysis of Thin Sections

Thin section no.	A_{su}	A_{sl}	A_{ln}	Porosity	Irreducible saturation
1	70.8(243)	29.2(100)	8.45(29)	40.5(153:62)	16.1(10)
	67.8(250)	32.2(119)	11.1(41)	45.5(154:70)	11.4(8)
2	79.8(253)	20.2(64)	3.5(11)	37.5(141:53)	3.8(6)
	78.3(252)	21.7(70)	6.5(21)	42.5(153:65)	4.6(3)
3	68.8(237)	31.2(107)	7.55(26)	36.6(156:57)	5.3(3)
	70.3(253)	29.7(107)	6.4(23)	29.4(143:42)	4.8(2)
4	71.8(267)	28.2(105)	7.25(27)	35.1(148:52)	7.7(4)
	74.6(294)	25.4(100)	4.55(18)	41.8(146:61)	4.9(3)
5	72.4(270)	27.6(103)	8.85(33)	43.6(149:65)	7.7(5)
	72.5(275)	27.5(104)	9.25(35)	36.5(145:53)	0.0(0)
6	67.4(269)	32.1(130)	7.25(29)	33.6(152:51)	7.8(4)
	66.7(263)	33.3(131)	7.6(30)	34.0(147:50)	2.0(1)
Av. values	71.6(3126)	28.4(1240)	7.4(323)	38.1(1787:681)	7.2(49)

EFFICIENCY OF DISPLACEMENT IN RANDOM PACKINGS OF EQUAL SPHERES

Data which relate solid surface area to work of displacement have been reported by Payne (*50*). Drainage curves for water displaced by air were measured for several random packings of equal spheres with sphere size varied from one packing to the next. Sphere surface area was measured directly by microscopic analysis. The work required to drain the spherical beads was almost equal to the product of the interfacial tension and the solid surface area of the beads. Average values of Payne's data are shown in Figure 16 as bead surface area versus work of displacement. These results appeared to indicate that, for a packing formed from spheres of a given size, work of displacement equals the increase in surface free energy of the system. The method has since received some acceptance as a general technique for determining the surface areas of coarse solids (*51*, *74*, *75*). However, the one-to-one relationship between surface area and work observed for random sphere packings is mainly coincidental. A critical assumption in evaluating the surface free energy of the drained bead pack was that essentially all of the solid surface had been exposed to the invading phase. In fact, the beads cannot be drained beyond their irreducible saturation; thus, some of the solid area must remain covered by wetting phase. Also, an interface exists between the discontinuous water and air which contributes to the total surface free energy of the drained bead pack. The following section describes experiments in which surface free energy changes were determined directly.

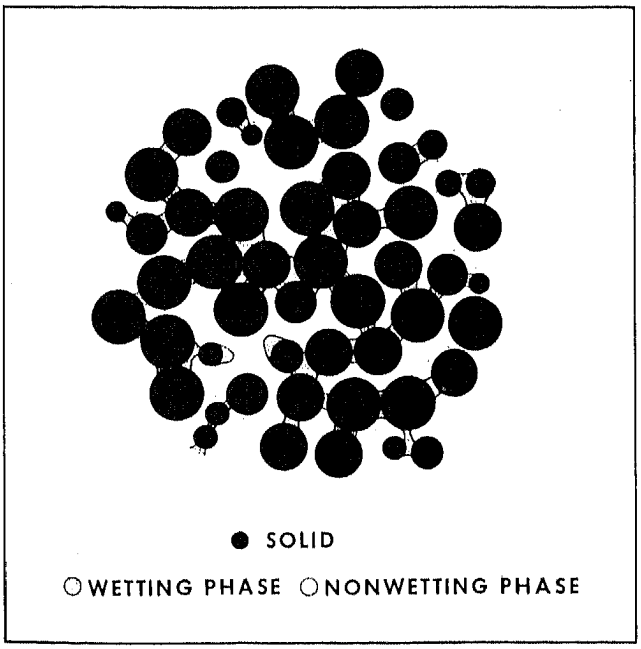

Figure 17. Distribution of fluid phases in a packing of 3 mm beads at the irreducible wetting phase saturation

Determination of Surface Areas at Irreducible Minimum Saturations

A random packing of 3-mm beads was held in a 1-1/2 in. diameter lucite tube with a supporting wire screen at one end. The column was saturated with a liquid epoxy resin containing a blue organic dye. The epoxy was allowed to drain by gravity. In the upper parts of the column liquid epoxy was retained as an irreducible wetting phase saturation. The blue epoxy hardened with very little shrinkage and occupied essentially the same position as when in the liquid state. The air space

in the core was evacuated and filled with an orange dyed epoxy resin primarily to strengthen the sample.

After the orange epoxy had hardened, six thin sections were prepared. They showed clearly the regions originally occupied by the spheres (transparent), the irreducible liquid epoxy saturation (blue), and the invading air (orange). Photographic enlargements were made directly from the thin sections. A drawing made from an enlargement is shown in Figure 17. On the enlargements, the region within about two particle diameters from the lucite wall was covered by a circular mask. A square grid was cast at random over the central region of the thin section photograph. Points on the grid were used to determine the relative fractions of space occupied by the solid spheres and the two colors of epoxy. The point count was used to determine porosity and saturation. Ratios of solid-liquid, solid-air, and liquid-air surface areas were determined by counting the number of times the lines on the grid intersected the various interfaces. Results are presented in Table IV. Surface areas are expressed as a percentage of the solid surface and are recorded as A_{sl}, A_{sa}, A_{la} where the subscripts, s, l, and a correspond to solid, liquid and air, respectively.

Bracketed figures in Table IV under columns labeled A are the number of line intersections for the indicated interface. The two bracketed numbers in the porosity column are the total number of points counted and the number lying within the pore space of the packing. Percentage porosity is calculated as the ratio of the second to the first. The bracketed figure in the irreducible saturation column is the number of points that fell in the region occupied by wetting phase. Although counts for individual thin sections resulted in fairly wide variations in porosity and irreducible saturation, the average values of 38.1% and 7.2%, respectively, are in close agreement with direct measurements of these quantities. Random packings of equal spheres usually have porosities in the range of 36–40% and irreducible saturations in the range of 6–8%. The average percentage of solid surface drained at the irreducible saturation was 71.6%, leaving 28.4% still covered by the liquid phase. The area of the air-liquid interface at the irreducible saturation was 7.4%.

An independent check of the fraction of solid surface which drains was made using a packing of 6-mm diameter ball bearings. The packing was saturated with a dilute acid and drained to its irreducible saturation. The retained acid etched the undrained region of the bearing surfaces. The bearings were dried, laid on a plane, and the uppermost point of each bearing used in point counting to obtain the ratio of drained to undrained surface. The result of 500 point counts indicated that 69.2% of the solid surface was drained; this value agrees substantially with the average value of 71.6% obtained from thin sections of the bead packs.

Efficiency of Initial Drainage

The liquid epoxy resin spread on glass; hence, the increase in surface free energy due to drainage should be

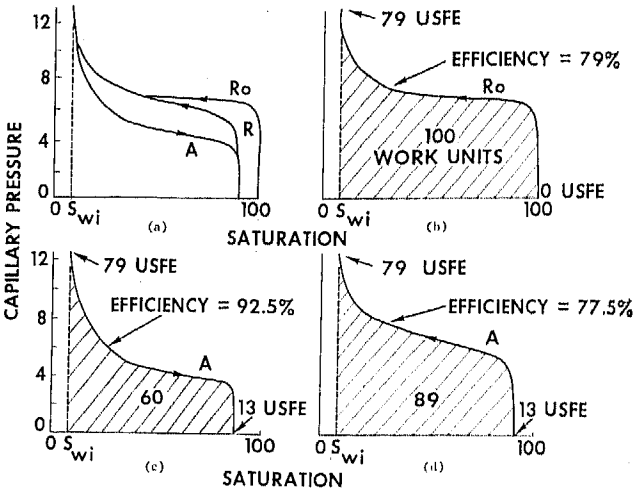

Figure 18. Relationships between work of displacement and changes in surface area for initial drainage, imbibition and secondary drainage (USFE = units of surface free energy)

directly proportional to the sum of the air-liquid and air-solid surfaces (cf. Equation 50). Expressing these areas as percentage units of the total solid surface, ΔF units of surface free energy,

$$\Delta \overline{F}_{(100 \rightarrow S_{wi})} = \Delta A_{sa}\,(71.6\%) + \Delta A_{la}\,(7.4\%) = 79\ USFE \quad (74)$$

The inherent efficiency, E_D of conversion of work to creation of surface is given by the increase in free energy divided by the work of displacement

$$E_D = \frac{\sigma_{la}(\Delta A_{sa} + \Delta A_{la})}{V_B\,\phi \int_{100}^{S_{wi}} P_c dS_w} \quad (75)$$

But from Payne's results shown in Figure 16, the work of displacement is equivalent in energy to the surface free energy of totally drained spheres. For purposes of comparing inherent displacement efficiencies, we can take the area under the capillary pressure initial drainage curve as 100 units of work and the surface energy of the totally drained solid (zero wetting phase saturation) as 100 units of surface free energy, equivalent to 100 units of work. (In general, the work given by the area under a capillary pressure drainage curve is not likely to be equivalent to the surface energy of any porous solid at zero wetting phase saturation.)

If the completely saturated solid is taken as a reference state for zero surface energy, then a drained bead pack will have 79 units of surface free energy at irreducible saturation. Since 100 units of work were required for drainage, the inherent thermodynamic efficiency of drainage from 100% saturation to S_{wi} is 79%. (See Figure 18b.)

Surface Area of Entrapped Nonwetting Phase

Determination of the inherent thermodynamic efficiency of imbibition requires measurement of residual nonwetting phase surface area. Gravitational effects in 3-mm beads are such that very little air is entrapped by

imbibition of a wetting liquid. Entrapment of air by liquid epoxy was therefore studied on two packings of microbeads. (The compressibility of air has little effect on the measured volume and surface area.) In one packing, bead diameters were in the range of 297 to 350 μ and in the other 125 to 149 μ.

A given packing was first saturated with liquid epoxy resin and then drained. The liquid epoxy was then imbibed into the packing and allowed to solidify. Attempts to prepare thin sections from packings of microspheres at residual nonwetting phase saturation were unsuccessful. Even in preparing a polished surface (which could only be examined by reflected light), portions of beads become dislodged during polishing; the resulting void spaces were not clearly distinguishable from entrapped air pockets.

The method finally chosen for preparation of a surface cross section was as follows. The packing was cut with a diamond saw, and the exposed surface was given a thick coating of red-dyed epoxy resin. After the resin hardened, it was ground away until the upper surface of the exposed packing had been lowered by a depth of about 2/3 of a bead diameter; this procedure removed the red-dyed epoxy which had filled spaces left by dislodged sphere segments. Examination of the exposed surface revealed the following distinguishable regions: (1) sphere segments or spherical bowls where sphere segments had broken away, (2) the blue epoxy of the originally imbibed wetting phase, (3) the red epoxy which had invaded pockets of air exposed when the sample surface was coated with red epoxy, and (4) air pockets (containing no red epoxy) which had been freshly exposed by grinding. The freshly exposed air pockets were relatively rare and generally distinct from spaces left by dislodged sphere segments. Finally, the surface was briefly exposed to hydrofluoric acid vapor which frosted the visible surface of bead segments to make them distinct when observed under reflected light.

To determine surface areas, the prepared cross section was examined with a binocular microscope using reflected light. The eye piece contained a 10 × 10 arithmetic grid. The objective was chosen so that one square on the grid was a little larger than one particle. For each line on the grid, the number of intersections with the solid surface and the number of intersections between the wetting phase and the nonwetting phase were counted. If grid lines cut positions where a nonwetting phase was touching the solid, it was counted both as a solid-liquid interface and as a liquid-air interface.

Results are shown in Table V. Six sets of measurements were made on the 297 to 350 μ bead packs. Only two measurements were made for the packing of 125 to 149 μ beads because of difficulty in obtaining sufficient illumination with reflected light. For the smaller bead packings, the surface area of the entrapped nonwetting phase was 13.8% of the solid surface and for the larger beads, 13.1%, to give an average overall count of 13.2%.

Work of Imbibition and Secondary Drainage

From surface areas determined thus far, efficiencies of imbibition and secondary drainage were obtained from respective areas under these curves. Results for three sets of capillary pressure tests on glass beads giving curves of the form shown in Figure 18a are presented in Table VI. The average area expressed as a percentage of the area under the initial drainage curve was 60% for imbibition and 89% for secondary drainage. These percentages are shown in Figure 18 as units of work.

Table V. Surface Area of Residual Nonwetting Phase as Percent of Total Solid Surface from Analysis of Thin Sections

Microbead diameter	Thin section no.	Counts ($A_{sa} + A_{sl}$), total solid surface	Counts ($A_{sa} + A_{la}$), residual nonwetting-phase surface	($A_{sa} + A_{la}$) as % of total solid area
297–350 μ	1	395	57	14.4
	2	390	55	14.1
	3	397	46	11.6
	4	393	58	14.7
	5	388	53	13.7
	6	401	40	10.0
All regions (1–6)		2364	309	13.1
125–149 μ	1	356	44	12.4
	2	342	52	15.2
Regions (1–2)		698	96	13.8
	Averaged values	3062	405	13.2

A = area, s = solid, l = liquid, a = air.

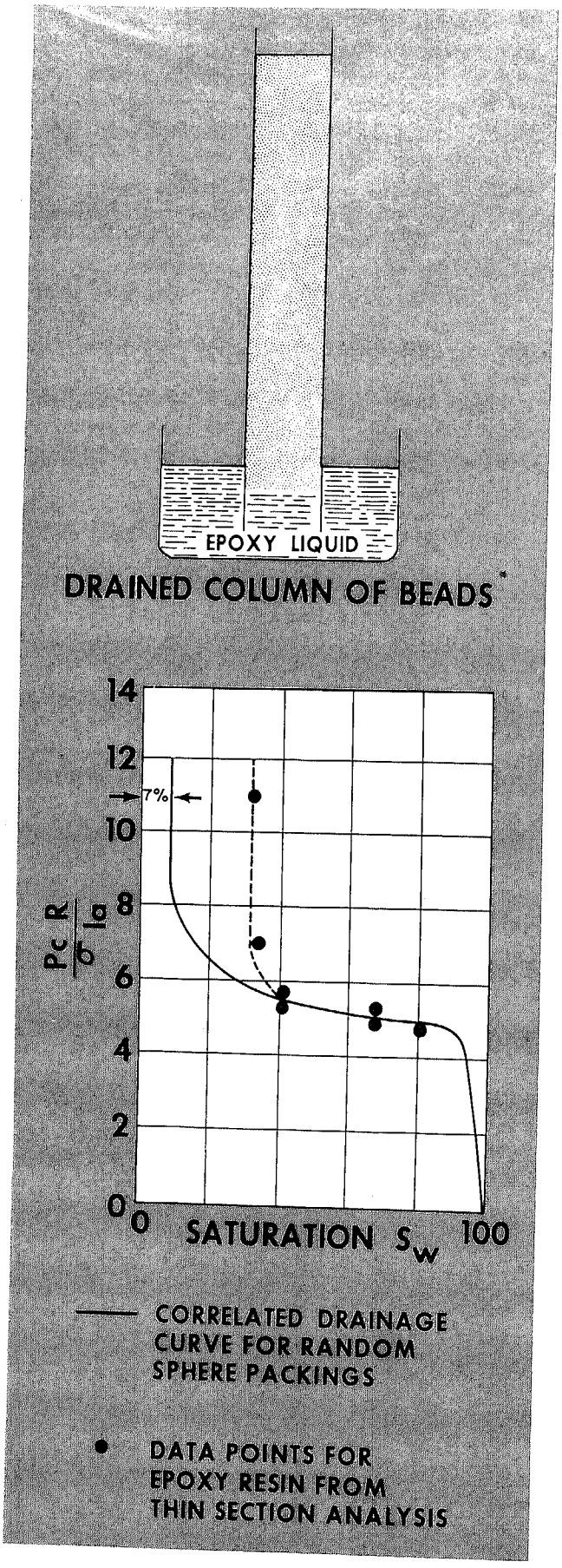

Figure 19. Distribution of solidified epoxy resin in a column of glass beads

Table VI. Percent Area under Capillary Pressure Curves Relative to Initial Drainage Curve

Microbead diameters, μ	Imbibition, A	Secondary drainage, R
250–297	62	92
177–210	63	85
177–210	56	90
Averaged values	60	89

Efficiency of Imbibition

Imbibition corresponds to the conversion of free surface energy of the porous system into external work. The area under the imbibition curve is about 60% of the area under the drainage curve (see Figure 18c). However, after imbibition is complete, the system still has surface free energy due to entrapped nonwetting phase equal to 13% of the solid surface. Adding the 60% for recovered work to the 13% for the stored surface energy, the imbibition efficiency is calculated as 73/79 or 92.5%; this value is considerably higher than the efficiency of initial drainage.

Efficiency of Secondary Drainage

The work required for secondary drainage is about 89% of that required for initial drainage. The initial surface free energy of the system was 13 units. Efficiency of secondary drainage can be defined as the ratio of the final surface free energy (79 units) to the sum of the initial free energy (13 units) and the work done on the system (89 units) to give a value of 79/102 or 77.5%. The presence of 13 units of residual nonwetting phase surface reduces the work of drainage by 11 units.

Displacement Efficiencies at Intermediate Saturation

Inherent thermodynamic efficiencies of displacement so far determined apply to maximum changes in saturation. To determine the efficiency of displacement at intermediate saturations, a column of 30–35 mesh microbeads was saturated with liquid epoxy resin and allowed to drain under gravity, as shown in Figure 19. Beads of this size give a transition zone of about 2 cm depth through which saturation should vary from nearly 100% to the irreducible saturation. After the epoxy had set, the space in the upper part of the column was evacuated and an orange epoxy injected under pressure and allowed to harden. Thin sections were prepared at one-half cm intervals along the length of the column and their saturation and surface areas determined by counting point and line intersections. Figure 20 is an illustration of part of a thin section in which both phases are mainly continuous. Analysis of the thin sections showed that epoxy had set in the upper region of the column before drainage to the irreducible saturation could occur. However, using the surface tension (38 dynes/cm) and density (1.1 g/cm^3) of the liquid epoxy and the average bead radius, R, a plot of $\Delta\rho ghR/\sigma_{1a}$ ($= P_cR/\sigma_{1a}$) *vs.* saturation approached a plot of P_cR/σ *vs.* saturation given by conventional capillary pressure drainage tests on sphere packings. Figure 19 shows the close agreement obtained for saturations above 35%.

The saturations and surface areas obtained by thin section analysis are summarized in Figure 21. In Figure 21, work of displacement at any saturation is expressed as percentage of the total work of displacement to irreducible saturation.

$$\text{work of displacement} = \frac{\int_{100}^{S_w} P_c dS_w}{\int_{100}^{S_{wi}} P_c dS} \cdot 100 \qquad (76)$$

The surface free energy is expressed as percentage of the total solid surface, A_s.

$$\text{surface free energy} = \frac{A_{la} + A_{sa}}{A_s} \cdot 100 \qquad (77)$$

Data points corresponding to irreducible saturation ($S_{wi} = 7\%$) are those obtained for the 3-mm diameter beads. The surface area between the fluid phases, shown in Figure 21, never exceeds about 10% of the solid surface. Since the surface area of residual nonwetting phase was 13%, the interfacial area between the fluids is probably about 10% at all stages of displacement.

Net efficiency, the ratio of increase in free energy to the work done, declines as the saturation decreases, Figure 21. A plot of net efficiency *vs.* saturation is shown in Figure 22.

Thermodynamic efficiency for a small displacement at a saturation S_w is given by

$$(E_D)_{S_w} = \frac{\sigma_{la} d(A_{la} + A_{sa})}{V_n \phi P_c dS_w} \cdot 100 \qquad (78)$$

The variation of $(E_D)_{S_w}$ with saturation is shown in Figure 22 as the stagewise efficiency curve. The inherent efficiency of conversion of work to surface free energy is highly nonlinear, declining from nearly 100% at high saturations to less than 60% near the irreducible saturation.

DISCUSSION

Techniques used in the present study could be extended to many other systems such as porous sedimentary rocks. Details of a solidified liquid technique for preparing thin sections illustrating fluid distribution in porous rock are reported by Le Fournier (*76*). Studies on other porous systems could determine whether the inherent thermodynamic efficiencies of drainage and imbibition found for random sphere packs are general or vary significantly from one rock sample to the next. Determination of changes in surface area of individual phases may find application in studies of both wettability and two-phase flow.

Wettability

Wettability of a porous medium relates to the surface energetics of displacement but is not a well-defined term. Capillary displacement pressures are often used as a measure of wettability; recently an empirical method of defining wettability according to ratios of areas under capillary pressure drainage and imbibition curves was presented by Donaldson, Thomas, and Lorenz (*77*). The present study also suggests that these areas provide a method of determining wettability if the inherent thermodynamic efficiencies of displacement and the surface areas of residual wetting and nonwetting phases are known.

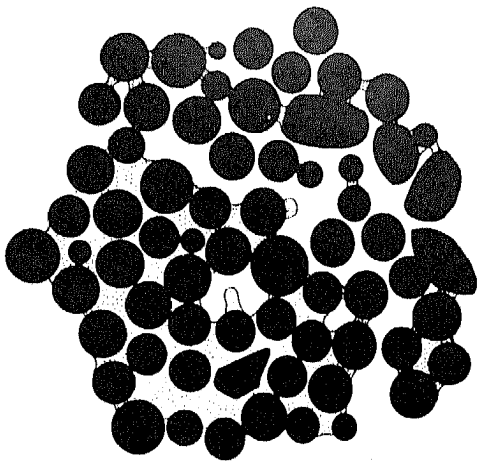

●SOLID ○WETTING PHASE ○NONWETTING PHASE

Figure 20. Distribution of fluid phases in a packing of 30–35 mesh microbeads when both phases are mainly continuous

If it could be assumed that the inherent thermodynamic efficiency of imbibition is always relatively high, then the work done by the system during imbibition might give an acceptable estimate of the surface free energy of the system at its irreducible saturation. A theoretical upper limit to the area under an imbibition curve would be largely determined by the product of the fluid surface tension and the contact angle integrated over the total exposed solid surface area. However, calculations of displacement pressures in sphere packings suggest that the inherent efficiency of imbibition will be considerably reduced when the contact angle is greater than zero (*67*). On the other hand, experimental studies of the effect of contact angle change with cubic shaped galena particles indicate that efficiency of imbibition may not change greatly with wettability (*78*).

The above observations point to fundamental difficulties that must be overcome in obtaining relationships among wettability, pore geometry, displacement pressures, work of displacement, and changes in surface free energy.

Fluid Flow—Hydraulic Radii of Individual Phases

The presented detailed mechanism of displacement is based on the assumption that capillary pressure data points are time independent and that capillary pressure curves correspond to infinitely slow displacement. Capillary pressure data are commonly used in solving equations of two-phase flow (*79*, *80*). Instances of distinct change in displacement mechanism with flow rate have been reported (*87*). For the present, we will assume that variations in the volume and surface properties shown in Figure 13 remain essentially unchanged.

Solutions to equations of flow also require relative permeability data for the two phases as a function of saturation. A variety of direct methods of measuring relative permeability have been described, mostly in soil science and oil production literature. Understanding of the mechanism of two-phase flow might be enhanced by comparing measured relative permeability to the volume and surface areas of individual flowing phases. Single-phase permeability of clean sands correlates well with hydraulic radius, r_h, given by the ratio of the volume of the pore space to the wetted surface area (*82, 83*). If ϕ is the porosity and A_s is the surface area of the solid per unit solid volume then,

$$r_h = \frac{\phi}{1-\phi}\frac{1}{A_s} \tag{79}$$

Darcy's equation for single-phase flow is:

$$\frac{dV}{dt} = \frac{kA'}{\mu}\frac{dP}{dL} \tag{80}$$

where dV/dt is the volumetric flow rate through a cross section, A', under pressure gradient dP/dL, μ is viscosity, and k is permeability.

The Kozeny-Carman equation incorporating hydraulic radius into the Darcy equation is usually written,

$$\frac{dV}{dt} = \frac{A'\phi r_h^2}{K\mu}\frac{dP}{dL} \tag{81}$$

The dimensionless parameter K, known as Kozeny's constant, usually has a value of about 5 for clean sands. If the surface area and porosity of a particle packing are known, permeability can be predicted from

$$k = \frac{\phi r_h^2}{5} \tag{82}$$

The concept of hydraulic radius has been extended to the flowing portions of the individual phases in two-phase flow (*52*).

Expressions for the hydraulic radius of individual phases are included in Figure 13. Only the continuous portion of each phase provides a flow path. The continuous portion of a flowing phase, say oil, is bounded mainly by the solid surface, $(A_{so})_c$. The remaining boundary of the continuous oil is given by the continuous oil-water surface and the oil-water surface of the discontinuous water. Thus, the hydraulic radius for oil, r_o, is given by

$$r_o = \frac{\phi S_{oc}}{(1-\phi S_{oc})}\frac{1}{[(A_{so})_c + (A_{wo})_c + (A_{\underline{wo}})_d]} \tag{83}$$

Data relating changes in surface area to saturation (Figure 21) permit calculation of r_o as a function of saturation for initial drainage from 100% saturation. Since all of the oil is continuous, S_{oc} is given by the oil saturation, S_o. The sum of the surface areas $(A_{so})_c$, $(A_{wo})_c$, $(A_{\underline{wo}})_d$ relative to the surface area of the solid can be taken directly from Figure 21.

The equation

$$\frac{dV_o}{dt} = \frac{A'S_{oc}\phi r_o^2}{K_o\mu}\frac{dP}{dL} \tag{84}$$

defines a parameter K_o analogous to the Kozeny constant K of Equation 81 for single-phase flow. The value of K is believed to reflect the tortuosity of flow paths within a porous medium. For displacements corresponding to a given capillary pressure curve, K_o probably varies with

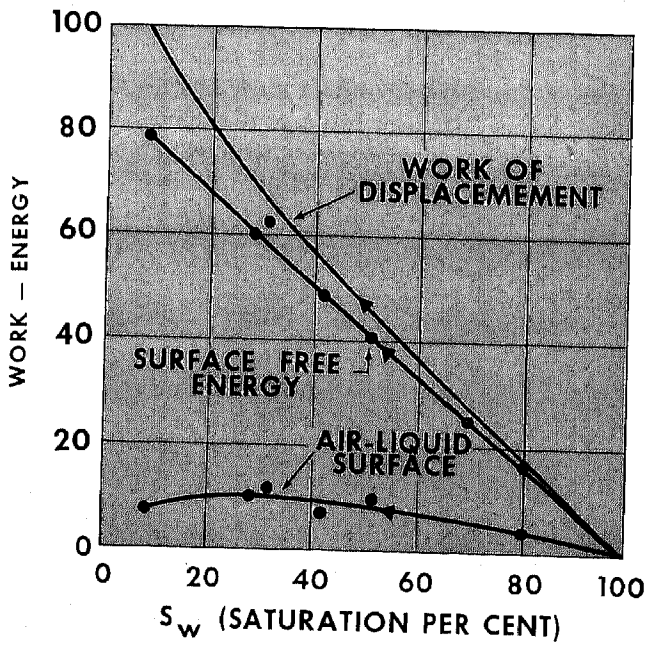

Figure 21. Relationships between work of displacement, surface free energy, and saturation for initial drainage

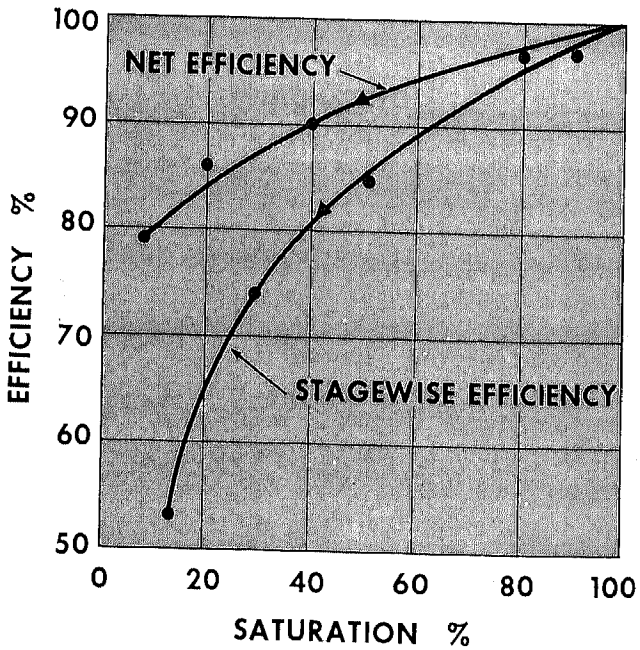

Figure 22. Net efficiency and stagewise efficiency versus saturation for initial drainage

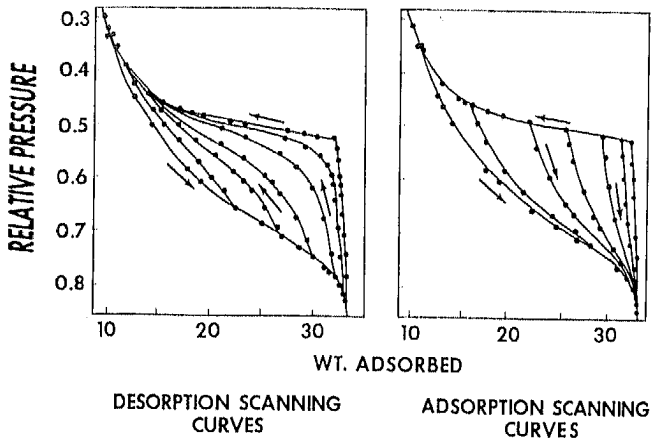

Figure 23. Hysteresis in sorption isotherms for xenon on porous glass at 751°K. (57)

saturation but this variation may similarly reflect changes in the tortuosity of flow paths available for the oil phase.

The value of K_o can be determined by comparing measured values of relative permeability k_{ro} with the hydraulic radius at a given saturation from the relationship

$$K_o = \frac{S_{oc}\phi r_o^2}{k_{ro}} \tag{85}$$

Relative permeability to oil, k_{ro}, is defined by

$$\frac{dV_o}{dt} = \frac{A'k_{ro}}{\mu}\frac{dP}{dL} \tag{86}$$

Equations 84 and 86 are equations of flow for individual phases and are analogous to Equations 81 and 80 for single-phase flow.

If both variations of K_o and displacement efficiencies are reasonably consistent, relative permeability could be predicted from capillary pressure data through Equation 85.

Hysteresis in Adsorption by Capillary Condensation

A number of general theories of hysteresis have been proposed. [See references cited by Everett (*56–59*).] A review of these theories and their relevance to the specific problem of immiscible displacement in porous media is beyond the scope of this paper. At present, no existing theory leads to accurate prediction of capillary pressure data. However, several observations of the present investigation bear importantly on the theory of hysteresis in adsorption by capillary condensation.

Hysteresis in adsorption isotherms, a topic recently reviewed by Everett (*57*), has been ascribed to several causes. Where the pore diameter of a solid adsorbent is large compared with the molecular diameter of the adsorbate, hysteresis has often been explained by capillary models. (When the solid has a high surface area, multilayer surface adsorption may contribute significantly to the total weight of adsorbed material (*84*); present considerations will be restricted to capillary condensate.) Striking similarities exist between the form of adsorption and capillary pressure hysteresis. (Compare Figures 8 and 23.)

Since adsorption isotherms represent a vapor in equilibrium with its liquid, all vapor-liquid curvatures are given by the externally measured vapor pressure. Whereas mass transfer across a phase boundary could be neglected for immiscible displacement, it dominates the mechanism of saturation change in adsorption. Thus, the distinction made between discontinuous and continuous fluid, defining stability conditions for capillary pressure data points, is unnecessary for adsorption. For example, a pendular ring of liquid held between two particles, after immiscible displacement, was assumed constant in volume, but the surface curvature and volume of capillary condensed liquid varies with vapor pressure.

Experimental observations of adsorption by capillary condensation are made in the range of capillary pressures where relative humidity is less than about 95% and vapor pressure varies significantly with surface curvature. Packings of spheres with diameters ranging from 100 to 1000 Å would provide suitable boundaries for the development of high surface curvatures. As a model, assume a sphere packing in which the absolute size of the spheres can be varied while maintaining similarity. If liquid is desorbed from this packing, essentially the same unstable configurations arise as in immiscible displacement, resulting in spontaneous movements of liquid. When vapor is adsorbed, the capillary mechanism differs somewhat from imbibition because isolated regions of fluid grow in volume as vapor pressure is increased, but imbibition and adsorption will still have comparable features. As with immiscible displacement, adsorption isotherms cannot be smoothly continuous on a microscopic scale.

A model proposed by Everett in discussion of macroscopic changes during adsorption (*57*) can also be used to discuss adsorption from a microscopic point of view as a quantized process (Figure 24). The adsorbent and adsorbate are contained in a cylinder, and vapor pressure can be changed by moving a frictionless piston. As in immiscible displacement, movement of the piston is only permitted when the vapor pressure is exactly balanced by the force on the piston. When an unstable configuration arises, the piston does not move until equilibrium is re-established. The force on the piston is then altered to balance the pressure of the vapor, and the piston continues displacement smoothly and reversibly until the next instability occurs. The area under the segmented pressure-volume curve so obtained is the reversible work done on the system. The increase in free energy of the system equals this work less the free energy lost during spontaneous transition. The size of the pressure change accompanying a transition is determined essentially by the factors that determined the pressure change associated with the rheons of immiscible displacement.

The hypothetical nature of this discussion is emphasized by the fact that these pressure changes for adsorption may be smaller than statistical fluctuations. However, as with rheons, the important feature of each

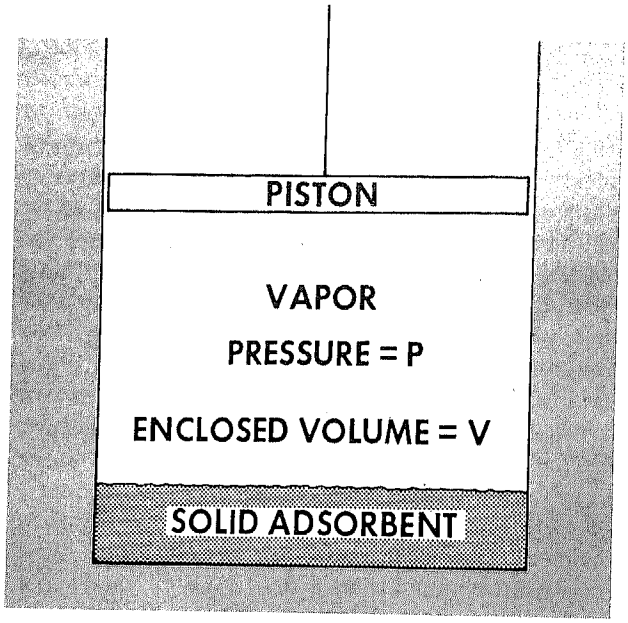

Figure 24. Idealized adsorption apparatus

instability is not the size of the pressure change, but the characteristic loss of surface free energy. This loss has a definite value as the pressure change approaches zero. As with capillary pressure hysteresis, the origin of hysteresis in adsorption by capillary condensation can be ascribed to the losses of surface free energy which accompany spontaneous changes of interface configuration. The simultaneous measurements of adsorption isotherms and surface areas reported by Wade and coworkers should permit calculation of inherent thermodynamic efficiencies of adsorption (*85*, *86*).

In seeking the origin of adsorption hysteresis, possible differences in the degree of irreversibility of adsorption and desorption isotherms have been investigated. Kington and Smith (*87*) made a calorimetric study of sorption of argon on porous glass. They concluded that adsorption occurred reversibly whereas desorption was accompanied by a spontaneous process. Although it does not seem likely that any one side of a hysteresis loop can actually correspond to reversibility, the above observation is consistent with the results of the present investigation in which imbibition was characterized by a considerably higher inherent thermodynamic efficiency than drainage.

REFERENCES

(1) Gibbs, J. W., "Scientific Papers," Vol. 1, pp 219–331, Dover, reprint, New York, N. Y., 1961.
(2) Haines, W. B., *J. Agr. Sci.*, 20, 97 (1930).
(3) Adam, N. K., "The Physics and Chemistry of Surfaces," 3rd ed., Oxford University Press, London, 1941.
(4) Herring, C., "Structure and Properties of Solid Surfaces," (Eds., R. Gomer, and C. S. Smith), University of Chicago Press, 1952.
(5) Shuttleworth, R., *Proc. Phys. Soc., London*, A, 63, 444 (1950).
(6) Pethica, B. A., and Pethica, T. J. P., Second International Congress on Surface Activity, Vol. III, Academic Press, New York, N. Y., p 151, 1957.
(7) Johnson, R. E., *J. Phys. Chem.*, 63, 1655 (1959).
(8) Gray, V. R., Discussion, Second International Congress on Surface Activity, Vol. III, p 192, Academic Press, New York, N. Y., 1957.
(9) Gray, V. R., *S.C.I. Monograph*, No. 25, p 123, London, 1967.
(10) Defay, R., and Prigogine, I., with collaboration of Bellemans, A., translated by D. H. Everett, "Surface Tension and Adsorption," Wiley, New York, N. Y., 1966.
(11) Gibbs, J. W., ref 1, p 219.
(12) Gibbs, J. W., *ibid.*, p 315.
(13) Gibbs, J. W., *ibid.*, p 237.
(14) Defay, R., and Prigogine, I., ref 10, p 61.
(15) Gibbs, J. W., ref 1, p 232.
(16) Tolman, R. C., *J. Chem. Phys.*, 17, 333 (1969).
(17) Melrose, J. C., IND. ENG. CHEM., 60 (3), 63 (1968).
(18) Defay, R., and Prigogine, I., ref 10, chap 17.
(19) Gibbs, J. W., ref 1, pp 314–15.
(20) Buff, F. P., and Saltsburg, H., *J. Chem. Phys.*, 26, 23 (1957).
(21) Gibbs, J. W., ref 1, p 326.
(22) Collins, R. E., and Cooke, C. E., *Trans. Faraday Soc.*, 55, 1602 (1959).
(23) Young, T., *Phil. Trans.*, p 65 (1805).
(24) Lester, G. R., *S.C.I. Monograph*, No. 25, p 123, London, 1967.
(25) Bailey, A. I., Discussion, Second International Congress on Surface Activity, Vol. III, p 189, Academic Press, New York, N. Y., 1957.
(26) Fowkes, F. M., "Surfaces and Interfaces I—Chemical and Physical Characteristics," Syracuse University Press, New York, N. Y., 1967.
(27) Gibbs, J. W., ref 1, p 328.
(28) Melrose, J. C., *J. Colloid Sci.*, 20, 801 (1965).
(29) Morrow, N. R., Discussion, Symposium on Wetting, *S.C.I. Monograph*, No. 25, p 210, 1967.
(30) Gibbs, J. W., ref 1, p 327.
(31) Fox, H. W., and Zisman, W. A., *J. Colloid Sci.*, 5, 514 (1950).
(32) Bikerman, J. J., Discussion, Second International Congress on Surface Activity, Vol. III, Academic Press, New York, N. Y., 1957.
(33) Melrose, J. C., *S.C.I. Monograph*, No. 25, pp 123–43, London, 1967.
(34) Harkins, W. D., "The Physical Chemistry of Surface Films," Reinhold, New York, N. Y., 1952.
(35) Henniker, J. C., *Rev. Mod. Phys.*, 21, 322 (1949).
(36) Low, P. F., *Advan. Agron.*, 13, 269 (1961).
(37) Deryagin, B. V. Ed., "Research in Surface Forces," Consultants Bureau, New York, N. Y., 1963.
(38) Buff, F. P., *J. Chem. Phys.*, 23, 419 (1955).
(39) Gibbs, J. W., ref 1, p 330.
(40) Laplace, "Mechanique Celeste," supplement to 10th book, 1806.
(41) Fisher, R. A., *J. Agr. Sci.*, 16, 492 (1926).
(42) Melrose, J. C., and Wallick, G. C., *J. Phys. Chem.*, 71, 3676 (1967).
(43) Melrose, J. C., *A.I.Ch.E. J.*, 12, 986 (1966).
(44) Erle, M. A., Dyson, D. C., and Morrow, N. R., Preprint 36A, 61st Ann. Meeting, A.I.Ch.E., Los Angeles (1968); *A.I.Ch.E. J.* (to be published).
(45) Croney, D., Coleman, J. D., and Bridge, Pamela M., *DSIR Road Research Laboratory Tech. Paper*, 24, HMSO, London (1952).
(46) Scheidegger, A. E., "The Physics of Flow Through Porous Media," Macmillan Co., New York, N. Y., 1960.
(47) Leverett, M. C., *Trans. AIME*, 142, 152 (1941).
(48) Calhoun, J. C., Lewis, M., and Newman, R. C., *Trans. AIME*, 186, 189 (1949).
(49) Brooks, C. S., and Purcell, W. R., *Trans. AIME*, 195, 289 (1952).
(50) Payne, D., *Nature*, 172, 261 (1953).
(51) Ringqvist, G., *Proc. Swedish Cement Res. Inst.*, Stockholm, 28 (1955).
(52) Rapoport, L. A., and Leas, W. J., *Trans. AIME*, 192, 83–98 (1951).
(53) Ksenzhek, O. S., Kalinovskii, E. A., and Tsyganok, O. P., *Russian J. Phys. Chem.*, 38, No. 11 (1964).
(54) Rootare, H. M., and Prenzlow, C. F., *J. Phys. Chem.*, 71, 2733 (1967).
(55) Crawford, F. W., and Hoover, G. M., *J. Geophys. Res.*, 71 (12), 2911 (1966).
(56) Everett, D. H., *Trans. Faraday Soc.*, 50, 1077 (1954); 51, 1551 (1955).
(57) Everett, D. H., "Adsorption Hysteresis in the Solid-Gas Interface," Marcel Dekker, New York, N. Y., 1967.
(58) Everett, D. H., and Smith, F. W., *Trans. Faraday Soc.*, 50, 187 (1954).
(59) Everett, D. H., and Whitton, W. I., *ibid.*, 48, 749 (1952).
(60) Poulovassilis, A., *Soil Sci.*, 93, 405 (1962).
(61) Philip, J. R., *J. Geophys. Res.*, 69 (8), (1964).
(62) Topp, G. C., and Miller, E. E., *Soil Sci. Soc. Amer. Proc.*, 30, 156 (1966).
(63) Enderby, J. A., *Trans. Faraday Soc.*, 51, 835 (1955); 52, 106 (1956).
(64) Morrow, N. R., and Harris, C. C., *Soc. Petrol. Eng. J.*, 5, 15 (1965).
(65) Smith, W. O., *Physics*, 4, 425 (1933).
(66) Weast, R. C., Ed., "Handbook of Chemistry and Physics," The Chemical Rubber Co., Cleveland, 1964.
(67) Melrose, J. C., *Soc. Petrol. Eng. J.*, 5, 259 (1965).
(68) Miller, E. E., and Miller, R. D., *J. Appl. Phys.*, 27, 324 (1956).
(69) Heller, J. P., *Soil Sci. Soc. Amer. Proc.*, 32, 778 (1968).
(70) Gibbs, J. W., ref 1, pp 242–52.
(71) Harris, C. C., and Morrow, N. R., *Nature*, 203, 706 (1964).
(72) Raimondi, P., and Torcaso, M. A., *Soc. Petrol. Eng. J.*, 4, 49 (1964).
(73) Pearce, K. W., and Donald, M. B., *Chem. Eng. Sci.*, 10, 212 (1959).
(74) Orr, Clyde, Jr., and Dallavalle, J. M., "Fine Particle Measurement," Macmillan Co., New York, 1959.
(75) Eisenklam, Paul, "Chemical Engineering Practice," Vol. 2, Solid State, Butterworths, London, 1956.
(76) Le Fournier, M. J., *Bull. Ass. Fr. Tech. Petrole*, No. 175, New Ser., 17 (1966).
(77) Donaldson, E. C., Thomas, R. D., and Lorenz, P. B., *Soc. Petrol. Eng. J.*, 9, 13 (1969).
(78) Harris, C. C., Jowett, A., and Morrow, N. R., *Trans. I.M.M.*, 73, 335 (1964).
(79) Muskat, Morris, "Physical Principles of Oil Production," McGraw-Hill, New York, N. Y., 1949.
(80) Collins, R. E., "Flow of Fluid Through Porous Materials," Reinhold, New York, N. Y., 1961.
(81) Handy, L. L., and Datta, P., *Soc. Petrol. Eng. J.*, 5, 261 (1965).
(82) Carman, P. C., *Trans. Inst. Chem. Eng., (London)*, 23, 150 (1937).
(83) Coulson, J. M., and Richardson, J. F., "Chemical Engineering," Vol. 2, Pergamon, London, 1955.
(84) Venable, R., and Wade, W. H., *J. Phys. Chem.*, 69, 1395 (1965).
(85) Wade, W. H., *ibid.*, 68, 1029 (1964).
(86) Ferguson, C. B., and Wade, W. H., *J. Colloid Sci.*, 24, 366 (1967).
(87) Kington, G. L., and Smith, F. S., *Trans. Faraday Soc.*, 60, 705 (1964).